International Journal of Remote Sensing

ISSN: (Print) (Online) Journal homepage: https://www.tandfonline.com/loi/tres20

Estimation of individual stem volume and diameter from segmented UAV laser scanning datasets in *Pinus taeda* L. plantations

Matthew J. Sumnall, Timothy J. Albaugh, David R. Carter, Rachel L. Cook, W. Cully Hession, Otávio C. Campoe, Rafael A. Rubilar, Randolph H. Wynne & Valerie A. Thomas

To cite this article: Matthew J. Sumnall, Timothy J. Albaugh, David R. Carter, Rachel L. Cook, W. Cully Hession, Otávio C. Campoe, Rafael A. Rubilar, Randolph H. Wynne & Valerie A. Thomas (2023) Estimation of individual stem volume and diameter from segmented UAV laser scanning datasets in *Pinus taeda* L. plantations, International Journal of Remote Sensing, 44:1, 217-247, DOI: 10.1080/01431161.2022.2161853

To link to this article: https://doi.org/10.1080/01431161.2022.2161853

Published online: 12 Jan 2023.

INTERNATIONAL JOURNAL OF REMOTE SENSING
2023, VOL. 44, NO. 1, 217–247
https://doi.org/10.1080/01431161.2022.2161853

Taylor & Francis
Taylor & Francis Group

Estimation of individual stem volume and diameter from segmented UAV laser scanning datasets in *Pinus taeda* L. plantations

Matthew J. Sumnall[a], Timothy J. Albaugh[a], David R. Carter[a], Rachel L. Cook[b], W. Cully Hession[c], Otávio C. Campoe[d], Rafael A. Rubilar[e], Randolph H. Wynne[a] and Valerie A. Thomas[a]

[a]Department of Forest Resources and Environmental Conservation, Virginia Polytechnic Institute and State University, Blacksburg, VA, USA; [b]Department of Forestry and Environmental Resources, North Carolina State University, Raleigh, NC, USA; [c]Biological Systems Engineering Department, Virginia Polytechnic Institute and State University, Blacksburg, VA, USA; [d]Department of Forest Sciences, Universidade Federal de Lavras, Lavras, Brazil; [e]Cooperativa de Productividad Forestal. Departamento de Silvicultura, Facultad de Ciencias Forestales, Universidad de Concepción, Concepción, Chile

ABSTRACT

The competitive neighbourhood surrounding an individual tree can have a significant influence on its diameter at breast height (DBH) and individual tree stem volume (SV). Distance dependent competition index metrics are rarely recorded in traditional field campaigns because they are laborious to collect and are spatially limited. Remote sensing data could overcome these limitations while providing estimation of forest attributes over a large area. We used unoccupied aerial vehicle laser scanning data to delineate individual tree crowns (ITCs) and calculated crown size and distance-dependent competition indices to estimate DBH and SV. We contrasted two methods: (i) Random Forest (RF) and (ii) backwards-stepwise, linear multiple regression (LMR). We utilized an existing experiment in *Pinus taeda* L. plantations including multiple planting densities, genotypes and silvicultural levels. While the tree planting density did affect the correct delineation of ITCs, between 61% and 99% (mean 86%) were correctly linked to the planting location. The most accurate RF and LMR models all included metrics related to ITC size and competitive neighbourhood. The DBH estimates from RF and LMR were similar: RMSE 3.05 and 3.13 cm (R^2 0.64 and 0.62), respectively. Estimates of SV from RF were slightly better than for LMR: RMSE 0.06 and 0.07 m^3 (R^2 0.77 and 0.70), respectively. Our results provide evidence that ITC size and competition index metrics may improve DBH and SV estimation accuracy when analysing laser-scanning data. The ability to provide accurate, and near-complete, forest inventories holds a great deal of potential for forest management planning.

ARTICLE HISTORY
Received 29 August 2022
Accepted 7 December 2022

CONTACT Matthew J. Sumnall msumnall@vt.edu Virginia Polytechnic Institute and State University, Department of Forest Resources and Environmental Conservation, 228 Cheatham Hall, Blacksburg, VA 24061, USA

1. Introduction

The United States' forest products industry is concentrated on the South (Alig and Butler 2004). Forests in the southern U.S. produce most of the nation's timber, and approximately one-sixth of the world's timber, while only being 30% of the nation's forestland (Wear and Greis 2002). Loblolly pine (*Pinus taeda* L.) plantation forests form a significant proportion of the forested land-cover in the southern U.S. In the early 2000s, there were over 12 million hectares of pine plantations in this region. Approximately 80% of the one million hectares of forest established annually is loblolly pine (McKeand et al. 2003). This land-cover is projected to increase to 22 million hectares by 2040, with associated increases in timber production (Wear and Greis 2002). Advancements in silvicultural management, in terms of tree improvement, nursery management, site preparation, weed control, and fertilization, have contributed significantly to the productivity of these plantations (Fox, Jokela, and Allen 2007). Detailed information on the structure and composition of these forests is required for the appropriate deployment of silvicultural inputs from them (Corona 2010; Pond, Froese, and Nagel 2014; Tinkham et al. 2018).

Accurate forest structure quantification is required for several forestry applications, including management, fire behaviour analysis, and carbon accounting. Forest managers need information describing tree geometry and spatial distribution, which includes stem count, diameter at breast height (DBH; 1.37 m), total tree height and merchantable stem volume at as fine a spatial scale as possible (Hilker, Wulder, and Coops 2008). Generally, with field measurements, only a subset of total tree heights are measured because these are time-consuming to acquire (Avery and Burkhart 2001; Kangas and Maltamo 2006). Forest structure is typically inventoried manually using a random or systematic sampling approach (Scott and Gove 2002). Logistics, site accessibility, robust measurement techniques, and the cost of labour constrain manual inventories (Randolph 2015). The use of such approaches represents spatially discontinuous measurements, which cannot capture the fine-scale variability of attributes, such as biomass, leading to large sources of uncertainty (Jenkins, Birdsey, and Pan 2001). The adoption of new data acquisition methods could therefore overcome these limitations while allowing for new information requirements in the future and in maintaining cost-efficiency (Fridman et al. 2014).

Local environmental conditions between individual trees, including intraspecific competition with a different genotype (e.g. Carter et al. 2020), or any other vegetation may influence tree growth in loblolly pine. Individual tree growth models can include a competition index designed to quantify the degree of competitive stress on individual trees in a stand. These indices represent a neighbourhood of trees that have a positive or negative effect on the growth of a single subject tree (Radtke, Westfall, and Burkhart 2003; Burkhart and Tomé 2012). Models using spatially explicit, individual-tree and competition information to estimate metrics, like basal area and DBH, have increased accuracy in comparison to models which only used individual tree metrics (e.g. Mailly, Turbis, and Pothier 2003; von Oheimb et al. 2011; Costa, Finger, and Hess 2018; Premer, Chhin, and Zhang 2021). Distance-dependent competition indices (CI), comparing focal tree metrics like DBH, total height and crown projection area with neighbouring trees, are available but using these indices requires significant investment in field collection and is computationally demanding (e.g. Hegyi 1974; Biging and Dobbertin 1992; Castagneri et al. 2008). Remote sensing data could effectively overcome these field measurement limitations in

capturing data necessary for the calculation of CIs while providing information for forest attributes over large spatial extents, which were previously impossible.

The analysis of remote-sensing data has been found to play a key role in many national forest inventory efforts (Barrett et al. 2016). Airborne laser scanning (ALS) and approaches integrating these with field measurements have seen operational use in several jurisdictions (Næsset 2014; White et al. 2017; White, Penner, and Woods 2021). The point-cloud available from ALS platforms has been used to estimate various forest inventory metrics in many different contexts (e.g. Hyyppä et al. 2017). ALS measures the three-dimensional (3D) distribution of vegetation within forest canopies (White et al. 2016). Recent improvements in unoccupied aerial vehicles (UAVs) make drone laser scanning (DLS) a viable remote sensing platform, which offers a combination of small-scale multi-temporal high-resolution data at low-cost (Rothmund, Vouillamoz, and Joswig 2017). Acquiring ALS data from conventional (piloted) aircraft and UAVs is technically similar but different in terms of operating altitude and spatial extent (Torres-Sánchez et al. 2015; Messinger, Asner, and Silman 2016; Hardin et al. 2019). Acquiring ALS data from piloted aircraft can be difficult, however, due to logistics, aviation regulations, and high costs, which make repeated forest inventories impractical (Wulder et al. 2012). DLS data can generally provide a greater pulse/return density in comparison to conventional ALS due to operating altitude (Lin et al., 2011). High enough point densities with returns from beneath the canopy have allowed for the classification of tree stems (Neuville, Bates, and Jonard 2021).

Automatic delineation of individual tree crowns (ITCs) is possible from small-footprint ALS data with a sufficient pulse density. To this end increasingly complex methods have been developed for this purpose (Kaartinen et al. 2012; Zhen, Quackenbush, and Zhang 2016). ITC delineation allows for direct comparison of ALS and field measurements (e.g. Popescu, Wynne, and Nelson 2003). Methods used to identify ITCs and their features are varied. Corte et al. (2020a) and Gyawali et al. (2022) demonstrated methods to estimate the total tree height either directly from the classified point-cloud or from a canopy height model. Height to the base of the live crown (HTLC) has been estimated by fitting a function through the binned return frequencies by height (Dean et al. 2009; Sumnall et al. 2016), via the application of 3D clustering methods (Arkin et al. 2021) or through statistical modelling (Liu et al. 2021). Other studies have statistically modelled individual tree metrics of DBH and/or stem volume using ALS derived ITC return distribution covariates as predictors (Silva et al. 2017; Corte et al. 2020b). Metrics relating to ITC size (e.g. HTLC, crown area and 3D crown volume) have also been used for this purpose (e.g. Yao, Krzystek, and Heurich 2012; Wu et al. 2015; Moe et al. 2020; Corrao, Sparks, and Smith 2022).

High pulse density ALS may provide spatially explicit and accurate tree metrics as long as the ITC delineations are accurate. It is unknown if the prediction accuracy of stem DBH and volume can be improved using DLS derived CI neighbourhood metrics. This study explored the feasibility of using DLS data for delineating ITCs and estimating both DBH and stem volume. The primary purpose of this research was to develop an approach which initially derives metrics related to the competitive neighbourhood around each tree and, secondly, to evaluate the impact of this method on the estimation accuracy if these metrics are used to predict stem DBH and volume. The objectives were:

(1) Implement our ITC method and validate it against field stem mapped data in stands with variable planting densities and crown architectures;
(2) Estimate and validate ITC size metrics (total tree height, HTLC and horizontal crown area);
(3) Calculate size and CI metrics for each ITC, then use these as model inputs to estimate DBH and individual tree stem volume; and
(4) Evaluate the accuracy of estimates of DBH and individual tree stem volume.

2. Datasets and methods

2.1. Study sites and field sampling

Our study sites were at Bladen Lakes State Forest (BL), located in the North Carolina Coastal Plain, USA (34°49′49.63″N, 78°35′18.52″W) and at Reynolds Homestead (RH), located in the Virginia Piedmont, USA (36°38′33.04“N, 80°9′16.77“W). Both sites were managed plantation forests exclusively containing loblolly pine. Both sites were established and maintained in support of research studies investigating the role of intensive management in optimizing loblolly pine production (Yáñez, Fox, and Seiler 2015; Yáñez, Seiler, and Fox 2017). The annual average temperature and precipitation for the BL site is 16.9°C and 1170.7 mm, respectively. The annual average temperature and precipitation for the RH site is 13°C and 1159.3 mm, respectively (Yáñez, Fox, and Seiler 2015).

Both sites were established in 2009 with a split–split plot experimental design with three (BL) or four (RH) replications of six loblolly pine genotypes, two silvicultural intensities (operational and intensive, Yáñez, Fox, and Seiler 2015) and three planting densities (Table 1; Yáñez, Seiler, and Fox 2017). The intensive silvicultural treatments at both sites consisted of complete weed control and fertilization for the first three growing seasons. The general layout of field measurement plots is illustrated in Figure S.1. There were 108 and 144 plots at BL and RH, respectively. All plots at BL had 63 trees (7×9). At RH, one block had 63 trees/plot and three blocks had 81 trees/plot (9×9). There were 6,804 and 11,016 trees at BL and RH, respectively. The genotypes maximized within group homogeneity and ensured different tree crown structures at each site, which consisted of six genotypes. Genotypes (four clones, one open-pollinated family and one control-mass-pollinated family, Yáñez, Fox, and Seiler 2015) were the split–split plot treatments.

Two Nelder (NE) trials (Nelder 1962; Namkoong 1965) were installed in 2009 at RH to evaluate a wide range of planting densities using the same genotypes used in the split–split plot design. As stem spacing and neighbourhood are critical components of CIs, data from the Nelder trials were included in the analysis to increase our sample size and increase variability in our dataset in terms of tree proximity and spatial arrangement beyond that found in the sample plots, with the ultimate aim of providing training data

Table 1. Field plot attributes for Bladen Lakes and Reynolds Homestead.

Stem planting density	Trees per hectare	Within row spacing (m)	Plot size (m^2)
Low	618	4.42×3.66	1019
Medium	1,236	2.21×3.66	510
High	1,853	1.47×3.66	339

Table 2. Field measurements of survival (percentage of total alive), mortality (number of dead trees) and total tree height statistics (mean, minimum, maximum and variance) for the sites (Nelder (NE), Bladen Lakes (BL) and Reynolds Homestead (RH)) and years used as the standard for the individual tree crown delineation and dimension estimates.

Site – Year	Stem survival (%)	Mortality (number of dead trees)	Height mean (m)	Height minimum (m)	Height maximum (m)	Height variance (m)
NE 2017	97.11	25	16.53	3.32	13.26	6.45
RH 2017	90.36	1062	10.00	1.68	13.90	7.30
BL 2017	84.91	1027	11.00	0.46	15.57	14.82
RH 2021	88.73	1242	10.10	4.36	21.43	16.02

for more robust predictive models. Each NE has 36 circular wedges and each wedge contained 12 trees, resulting in planting densities from 227 to 7,142 trees ha^{-1} and a total of 864 trees (2 Nelders × 36 wedges × 12 trees), illustrated in Figure S.2. There were no Nelder trials located at the BL site.

We acquired the GPS location of each tree in all locations in 2009 immediately after planting. In January 2017, we measured all trees at BL, RH and NE. In early January 2022, we measured all the RH trees (RH 2021). For all trees, we measured DBH (at 1.37 m) and survival. The presence of standing or fallen dead stems was recorded. For all NE trees and for the 25 (5 × 5) trees in the centre of each plot at BL and RH, we also measured the total tree height, HTLC and crown diameter. Total tree heights were measured with a Vertex hypsometer, with a measurement error of 0.2–0.3 m (Vasilescu 2013). Height and stem survival are summarized in Table 2. HTLC was defined here as the vertical distance between the ground and the lowest live branch. Two horizontal crown diameter measurements were taken along perpendicular axes centred on the tree stem: (1) within and (2) across planting rows (Bechtold and Randolph 2018). The crown edge was the perimeter of the visible crown from the ground. Measurements were made at ground-level with a tape measure held from crown edge-to-edge drip lines. We assumed that the horizontal crown area, or projection area, was approximately elliptical given the rectangular planting densities and high degree of canopy closure in our study sites. Thus, we approximated this as the area of an ellipse ($\pi \times$ diameter 1 × diameter 2). Mortality, total height and DBH measurements were available for 11,628 stems. Merchantable stem volume was calculated using the unthinned over-the-bark model from Tasissa, Burkhart, and Amateis (1997).

This model is expressed as:

$$V_{ob} = 0.21949 + 0.00238 \times D^2 \times H \quad [1]$$

where V_{ob} is the total outside bark volume (in cubic-feet), D is DBH (in inches) and H is the total tree height (in feet).

2.2. DLS data acquisition and pre-processing

Discrete return DLS data were acquired in April 2017 for RH and NE and in August 2017 for BL. The UAV platform was a Vapour-35 helicopter (AeroVironment, Simi Valley, CA, USA) with a YellowScan Surveyor Core LiDAR unit (Montferrier-sur-Lez, France). The DLS unit consists of a Velodyne VLP-16 laser scanner (Velodyn, 2019) and a GNSS-inertial Trimble

APPLANIX APX-15 (Trimble, Richmond Hill, ON, Canada). The DLS system recorded up to two returns per laser pulse and used a near-infrared (NIR) wavelength of 905 nm, over approximately 1 km^2 separately for each site. Pre-processing and strip adjustment was conducted before DLS data processing in the YellowScan CloudStation software. Data specifications were:

- a laser pulse density of 312 to 498 pulses m^{-2} from combined flight lines;
- ≤60° scan angle on either side of nadir;
- A flight altitude of 50 m (RH and NE) and 60 m (BL) – relative to take-off location;
- A 50% overlap between flight lines;
- 300 kHz laser pulse repetition rate;

Ground control for the 2017 DLS acquisitions used a real-time kinematic geographic positioning system (RTKGPS, Topcon GR-3) with precision ≤10 cm and positional accuracy ≤5 cm.

The DLS data were acquired for RH 2021 in July 2021 using the DJI M600 hexacopter platform (DJI Technology Co. Ltd., Shenzhen, China) with a Riegl MiniVux1 LiDAR scanner (RIEGL Laser Measurement Systems GmbH) and APPLANIX APX20 GNSS-inertial measurement unit (Trimble, Richmond Hill, ON, Canada). The DLS system recorded up to six returns per pulse and used a near-infrared (NIR) wavelength of 905 nm, over approximately 1 km^2 covering the same spatial extent as in 2017. Pre-processing and strip adjustment were conducted before DLS data processing in the RiPROCESS software (RIEGL Laser Measurement System GmbH, Horn, Austria). Data specifications were:

- a laser pulse density of 700 to 1011 pulses m^{-2} from combined flight lines;
- ≤85° scan angle either side of nadir;
- A flight altitude of 60 m – relative to take-off location;
- An 80% overlap between flight lines;
- 100 kHz laser pulse repetition rate;

Ground control for the 2020 acquisition used a RTKGPS (Spectra SP80) with a post-processed positional accuracy ≤0.3 cm.

DLS data pre-processing and analysis was completed using R software (version 4.1.1.) (R Core Team 2021). The lidR (version 4.0.0, Roussel et al. 2020; Roussel and Auty 2022) and data.table (version 1.14.2, Dowle and Srinivasan 2021) packages were used on LAS format files. The following packages were used for geographic information system functions, sp (version 1.4–6, Bivand, Pebesma, and Gomez-Rubio 2013), sf (version 1.0–7, Pebesma 2018), rgdal (version 1.5–29, Bivand, Keitt, and Rowlingson 2021) rgeos (version 0.5–9, Bivand and Rundel 2021), maptools (version 1.1–3, Bivand and Lewin-Koh 2022) and raster (version 3.5–15, Hijmans 2022). The dbscan package (version 1.1–10, Piekenbrock and Doran 2019) was used for clustering points based on relative distance to their neighbours and noise removal. The MASS package (version 7.3–55, Venables and Ripley 2002) was used for 2D kernel density analysis. The soilphysics package (Silva and Lima 2017) was used to assess graph-slope curvature. The deldir package (version 1.0–6, Turner 2021) was used for the creation of Voronoi tessellations. The geometry package (version 0.4.5, Habel et al. 2019) was used for the calculation of 3D convex-hulls. Statistical analysis was

conducted using the Boruta (version 7.0.0, Kursa and Rudnicki 2010) and caret (version 6.0–91, Kuhn 2021) packages.

LAS file pre-processing began with noise removal, where return-points were classified using an isolated voxels filter. The following settings were determined visually as the most effective after testing a number of permutations. A 3D matrix was created for the extent of each LAS file, where voxels were cubic and had a side length of 1 m. A search kernel of $3 \times 3 \times 3$ was created. Returns were classified as noise if only one return was located within the search extent. Ground-returns were classified by the implementation of the Cloth Simulation Filter (Zhang et al. 2016). Aboveground heights were calculated by first creating a surface from ground-classified returns, using a triangular irregular network, and this height was then subtracted from all non-ground returns.

2.3. Individual tree crown delineation

We developed a new method to identify likely tree stem locations, which exploits the high pulse density, the increased probability of pulses returning from vertical surfaces due to scan angle, and the penetration of pulses through the canopy. The process is summarized in Figure 1.

The following approach was inspired by the Height-Scaled Crown Openness Index (HSCOI), which provides a 2D quantitative measure of ALS pulse penetration through the

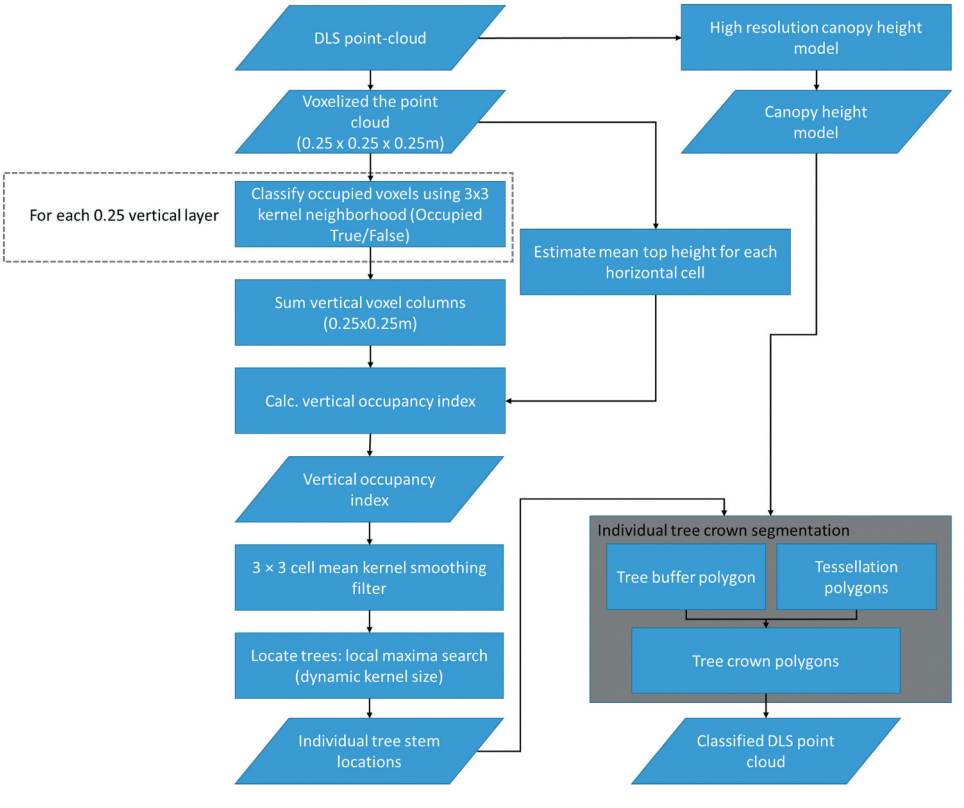

Figure 1. Flowchart of the DLS data processing for classifying individual tree crowns.

canopy (Lee and Lucas 2007). The HSCOI aids in locating tree stems in the overstory and sub-canopy of multi-layered forests. Our high pulse-density data provided a high probability of returns coming from stems, and we developed a similar method to represent 3D space occupancy, which is described in the following.

This process was performed on all four datasets/sites independently. We created a 3D matrix of $0.25 \times 0.25 \times 0.25$ m voxels from the DLS point-cloud. A voxel was created if there was at least one return within the 3D extent of the voxel cell (Figure 2a). The voxel occupancy index (VO_{index}) was calculated horizontally across the DLS acquisition extent and expressed as a proportion (0–1) for each vertical, 0.25 m layer. If an occupied voxel existed within a 3×3 voxel horizontal kernel, then the voxel was considered occupied (Figure 2b). The number of occupied voxels was summed vertically ($Vox_{presence}$), and this value was multiplied by the voxel vertical extent (Vox_{size}, 0.25 m).

The calculation was:

$$VO_{index} = \frac{Vox_{size} \times \sum_{n=1}^{n_{voxels}(i)>0} Vox_{presence}}{\max ht_{local}} \quad [2]$$

where $max\ ht_{local}$ was the maximum DLS return height within a search radius of 10.4 m (from the voxel horizontal centre). This search radius was determined from the smallest field plot area (339 m^2). We created a raster surface using this approach with a spatial resolution of 0.25×0.25 m.

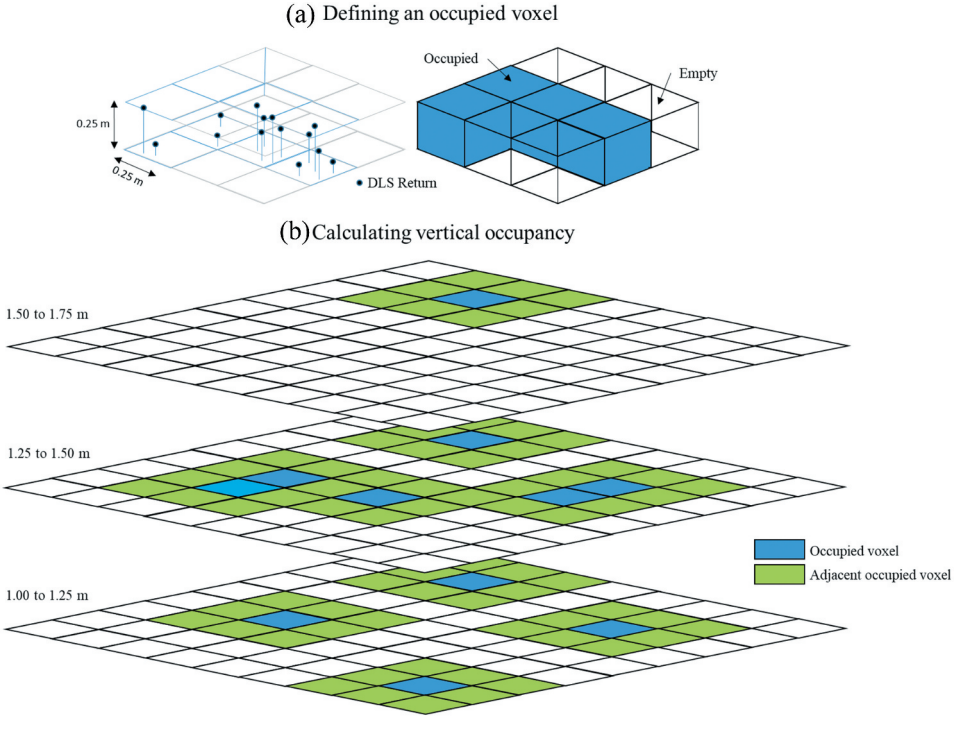

Figure 2. An example determining an occupied voxel (a) – where a voxel cell was considered occupied if one or more LiDAR returns came from within its extent. Occupancy of the 0.25 m vertical layers (b) were computed independently. Voxels were considered occupied if they had LiDAR returns in the voxel (blue), or if that voxel was directly adjacent to an 'occupied' voxel (green).

Prior to the tree delineation, a 3 × 3 cell mean kernel-smoothing filter was applied to the VO_{index} raster layer to reduce noise and false positives (as in Popescu, Wynne, and Nelson 2003). Higher VO_{index} values were associated with the locations of tree stems or dense clumps of vegetation located within large tree crowns. A variable search window local maxima filter was implemented to locate likely tree centre locations (Roussel et al. 2020), which is determined by the VO_{index} value. After experimenting with 33% of BL field measurements, we created a polynomial formula where large windows were created for small index values, and vice versa for large index values, and is expressed as follows:

$$window_{size} = 0.0006 \times (VO_{index} \times 100)^2 - 0.1075 \times (VO_{index} \times 100) + 6 \quad [3]$$

where $window_{size}$ is the diameter of a circular search kernel, with units in metres. If maxima were located within 1 m horizontally, they were merged, keeping the location of the larger VO_{index} value (e.g. Figure 3).

We created a high-spatial-resolution (0.1 × 0.1 m) CHM from the point-cloud using the digital surface model algorithm (Roussel et al. 2020). The method of delineating ITC horizontal polygon boundaries was implemented as defined in Silva et al. (2016). The method delineates ITCs based on a segmentation of the CHM using initial markers (tree stems derived from the VO_{index}), and the comparison of two polygon areas is then completed. Firstly, a variable radius polygon, depending on height, is established around each tree centre. These polygons were then split using centroidal Voronoi tessellation, generating polygons of the ITC horizontal extents. The DLS point cloud was then classified into individual trees using this polygon layer. Any ITC with a top height of <4.7 m was

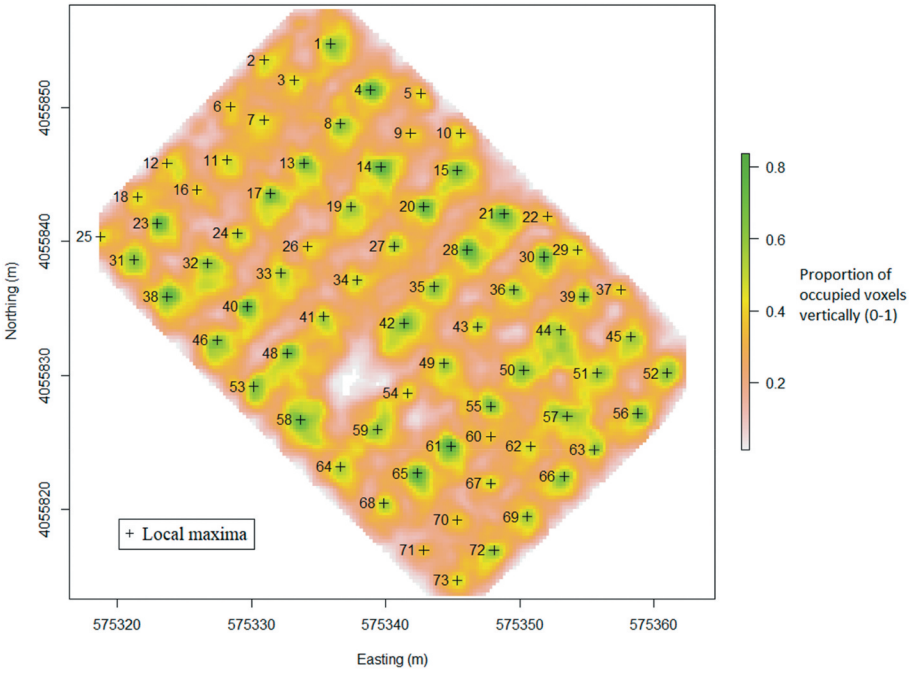

Figure 3. A VO_{index} raster generated for a single sample plot. Local maxima are illustrated. Stem spacing was 4.42×3.66 m.

considered as understory vegetation, given previous research in proximity (Sumnall et al. 2017), and removed.

2.4. Individual tree crown metrics

The DLS point cloud was subset by ITC classification, and each was considered as independent. Each of the following metrics was indented as model input variables to predict stem DBH and volume. We determined tree position as a mean of X and Y coordinates of returns classified to a specific ITC assuming the stem was straight and vertical. The total tree height was the tallest returned pulse. The crown area was calculated using a horizontal convex hull derived from all returns >1 m (as in Vauhkonen et al. 2014). ITC crown horizontal diameter was calculated from the largest uninterrupted distance from one side to the other after converting the convex-hull into a polygon.

We estimated HTLC using a modified version of the Sumnall et al. (2016) method. This approach was developed using a random 10% of the linked field and DLS ITC dataset for RH 2017, which was then applied to the remaining dataset. Classified returns for each ITC were considered independent and processed separately. The ITC subset of returns aboveground (>0.2 m) were separated into 0.2 m height bins (0.2–0.4 m, 0.4–0.6 m, etc.) and returns were summed within each bin. A minimum return frequency baseline was calculated as 30% of the sum of all returns divided by the total number of bins, similarly to that implemented in Holmgren and Persson (2004). A cubic smoothing spline was then fit to the distribution of the return frequency by height using a smoothing parameter of 0.5. Local maxima and minima were identified on this line. Maxima were excluded if they were below the baseline value. The maxima were classified as from the canopy if they satisfied the following criteria: (i) above one-third tree height and (ii) frequency values must be larger than 45% of the largest frequency-bin value. The maxima with the lowest height fulfilling the above criteria were classified as being the lowest maximum which was part of a pine crown. The minimum directly below this canopy maximum was considered the initial estimate of the HTLC (Figure 4); however, as in Sumnall et al. (2016), this minimum could underestimate HTLC. HTLC estimations were refined to address this underestimation with the following algorithm:

(1) The height-bins corresponding to the lowest-canopy maximum and the minimum directly beneath it were subset where X was the return frequency, and Y was the height above ground;
(2) If the frequency-of-returns value corresponding to the canopy minimum was lower than the baseline value, all of the height-bin values below the lowest-canopy maximum were subset;
(3) If the vertical distance between the tallest and lowest height-bins was greater than or equal to 3 m, a cubic-spline was fit to these height-bins (using the above specifications). Then, a new HTLC was calculated as follows:
    (a) The point on the curve where the curvature was at its maximum was calculated using the soilphysics package maxcurv function (Da Silva and De Lima, 2017). This height was then considered to be the HTLC;
    (b) Otherwise, the HTLC was unaltered.

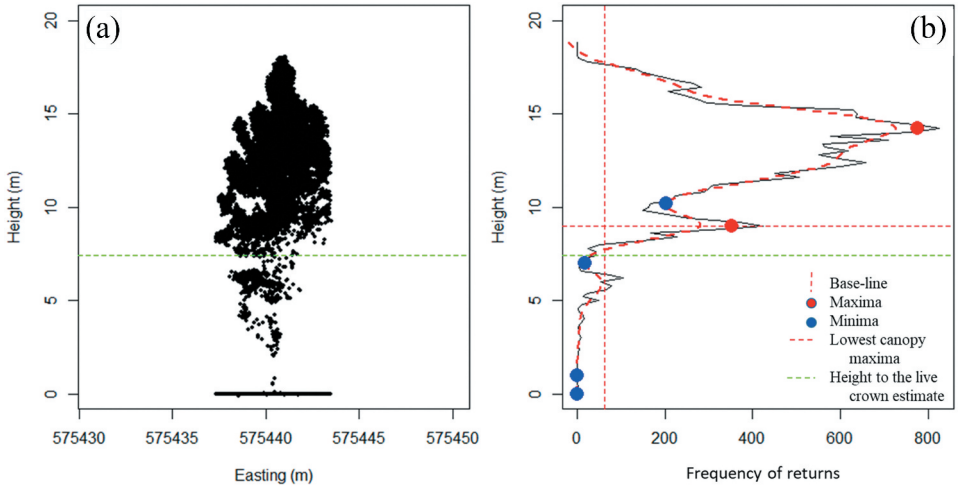

Figure 4. A profile view of the classified returns for a sample ITC (panel A). The frequency of returns by height (panel B) and the identification of the lowest canopy feature and estimate of height to the living crown.

Finally, a 2D kernel density raster was created for the ITC-classified return's X and Z coordinates using the kde2d function in the MASS package. All rasters were created with 100×100 cells. Local raster maxima were identified using a 5×5 cell kernel moving window. Raster maxima less than 10% of the largest value were removed. If there were any raster-maxima below and within 1 m vertically (Z coordinates) of the initial HTLC estimate, then the height minimum immediately below this raster-maximum was selected as the new HTLC value.

In order to calculate metrics related to 3D crown volumes (as in Korhonen et al. 2013) and surface areas, ITC subset returns were further subset to give datasets containing all of the returns in the top 10%, 20%, 30%, 40% and 50% of tree height. A 3D convex-hull was fit to each of these point-cloud subsets using the geometry package. A total of 10 3D crown volume and the surface area of the hull metrics were calculated and used as ITC model inputs.

In addition, ITC leaf area index (LAI) was calculated using the method documented in Sumnall et al. (2021). As in the aforementioned study, all returns with scan angles above 30° were discarded. The above below ratio index (ABRI) method was used and can be expressed as:

$$ABRI = \frac{\sum R_{>T}}{\sum R_{\leq T}} \quad [4]$$

Where, R denotes an individual DLS return and T represents a height threshold, of which returns are excluded if under or over this height, which, in this case, was set to the estimates of ITC HTLC. Regression model coefficients were the same as those determined in Sumnall et al. (2021).

2.5. Calculating individual tree crown competition neighbourhood metrics

Several approaches to define the horizontal or vertical competitive zone for a given tree were available (Weiskittel et al. 2011). The key in determining tree competitive zones was understanding that each tree has an area where it obtains or competes for resources (Bella 1971). Competition for each tree was assessed by the degree of overlap between competitive zones. Consequently, here we defined this as trees immediately neighbouring one another and assumed that the closer trees were to a given focal tree, the greater the competition for resources. A given ITC/focal tree, and a typical rectangular arrangement, could have up to eight neighbours; however, we had variations due to differences in tree spacing and missing stems from mortality. To manage these issues, we needed to classify the neighbours for each ITC automatically. The competitors for a given ITC/focal tree were the surrounding ITCs, in terms of proximity and direction. Voronoi polygons were generated from the ITC centre coordinates such that each polygon defined an area of influence around its centre coordinates, so that any location inside the polygon was closer to that ITC centre than any of the other ITC centres. Polygons touching the subject polygon were the initial set of competing neighbours (Figure 5). This process may not account for all competing neighbours, so the distance and azimuth from the subject ITC to potential neighbour coordinates were calculated. If there was a gap of over 20° between current neighbours, we searched for and added additional ITC points within 10 m from within that azimuth angle range (see Figure 5). If there were multiple potential neighbours within the 20° azimuth, the closest ITC was preserved, and the others removed. Horizontal distances were calculated for all neighbours to each ITC coordinate.

We adapted two approaches to calculate CI from DLS derived ITC data using the automatically defined neighbourhoods. First, we used Hegyi's distance-dependent competition index (DCI) (Hegyi 1974):

$$DCI_i = \sum_{j=1}^{n} \left(\frac{D_j}{D_i} \times \frac{1}{DIST_{ij}} \right) \quad [5]$$

where D_i, was DBH of the subject tree i, D_j was DBH of competitor tree j and $DIST_{ij}$ was the distance between trees i and j in metres. Instead of using DBH as the primary variable, we calculated a CI using each of the metrics defined in section 2.4: total tree height, HTLC, horizontal crown area, crown horizontal diameter, five 3D crown volume metrics (for the top 10, 20, 30, 40 and 50% of the total height), and five 3D crown surface area metrics (for the top 10, 20, 30, 40 and 50% of height). A total of 14 CI metrics for each ITC were calculated. The number of neighbours identified was also recorded.

Second, we used an adapted version of the single tree-based stand simulator (SILVA) to explicitly identify neighbours relative to the subject tree based on 3D position (Pretzsch, Biber, and Ďurský 2002). This index calculated a 3D cone where the apex was at the live crown base, and the cone base faced up. Cone size was calculated where the apex angle was 30° and cone height was the same as total tree height. Treetop coordinates intersecting with this cone were the competitive neighbour crowns, which were summed:

$$SILVA2_i = \sum_{j=1}^{n} \beta_j \times \frac{CCA_j}{CCA_i} \quad [6]$$

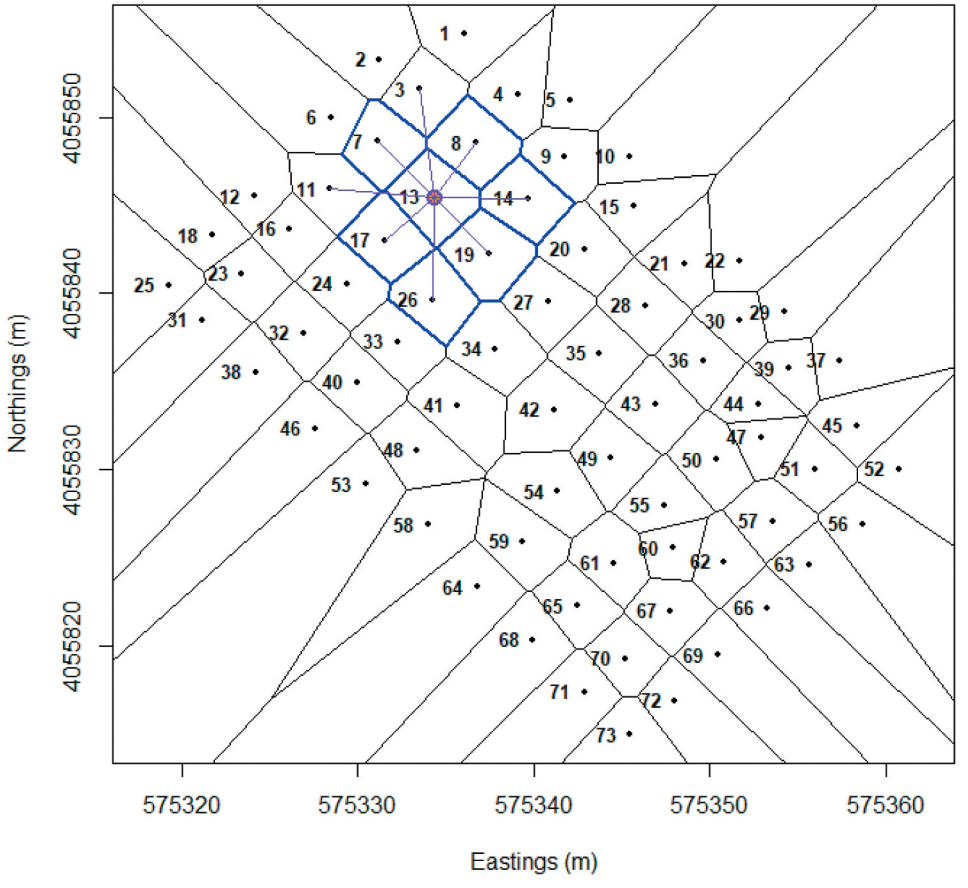

Figure 5. Voronoi polygons created for a sample single plot extent, created from ITC center coordinates. All potential immediate touching neighbor polygons for ITC ID 13 (purple) are indicated in blue. Additional neighbor IDs of 3 and 11 were identified based on proximity and angle gaps (with regard to immediate neighbors).

Where, $SILVA2_i$ was the CI for tree i, β_j the angle between cone vertex and top of competitor j, CCA_j, CCA_i the crown cross-sectional area of trees j and i, respectively, and n the number of competitors of tree i. The original equation included a term for the species-specific light transmission coefficient for tree j which was not applicable here (Ellenberg 1996). We calculated the number of neighbouring crowns and the index value for each ITC.

2.6. Linking field and DLS individual tree crown metrics

To determine the tree position, we assumed the stem was straight and used the centre of gravity coordinates calculated for each ITC. Tree GPS coordinates were compared directly with DLS delineated ITC objects as follows. A 1 m radius buffer was applied to the GPS planting location, and we examined ITC coordinates that intersected this polygon and linked the ITC with the coordinates closest to the GPS centre. Only one ITC could be linked to a GPS location. Presence, total tree height, and crown dimensions were compared with field data. If a planting GPS location was

not linked to an ITC coordinate, it was counted as an omission error, unless it was recorded as dead in the field data. ITC objects linked to standing dead stems were considered as correct but were excluded from statistical analysis. Here, we defined an error of omission as an error in which an ITC cannot be linked to a field tree planting location. An error of commission was defined as the error in which more ITCs have been delineated than can be reasonably accounted for using field data.

2.7. Statistical analysis

Our goal was to develop a method for estimating DBH and stem volume. Consequently, we attempted two approaches: (i) Random Forest (RF) and (ii) backwards-stepwise, linear multiple regression (LMR). Linear regression methods are inferior to machine learning in describing structurally complex forests (Chen and Hay 2011); however, machine learning approaches do not extrapolate well beyond the range of the training dataset. To specifically test if the inclusion of CI metrics improves prediction accuracy, two additional permutations of analyses were implemented, where statistical analyses were performed with (i) only tree size metrics (total height; crown horizontal area; crown horizontal diameter; HTLC; LAI; five crown volumes; and five crown surface area metrics); and (ii) including both tree size and CI metrics.

The RF model (Breiman 2001) uses an ensemble method to perform classification or regression tasks (e.g. Yu et al. 2011; Wu et al. 2015; Silva et al. 2017). We implemented this method twice, in the first iteration only ITC size metrics were used (13), whilst the second used a combination of ITC size and CI metrics (30) as predictor variables. To estimate DBH and stem volume, we had 29,700 and 11,628 individual tree field measurements, respectively, between the two sites and measurement years (RH and BL, 2017 and 2021). These datasets were randomly subset into training and validation sets, accounting for 75% and 25% of the sample size, respectively. The number of DLS ITC metrics was large; consequently, we implemented a variable selection and reduction approach to ensure modelling within a parsimonious statistical framework. We used the Boruta R package, a wrapper built around the RF algorithm (Kursa and Rudnicki 2010), to assess the relative importance of 30 predictor metrics. This approach duplicates and reshuffles the training dataset and implements an RF classifier, up to 500 times, and predictor accuracy/impurity was assessed with a Z-score. The approach compares Z-scores at each iteration and marks it as important if it outperforms its duplicate. At the end of this process, the six most important predictor variables (if available) were used as input into the RF model.

We used the caret R package for RF model tuning and construction. Tuning with a 10-fold cross-validation control determined the optimal value for the number of variables randomly sampled as a candidate RF tree branch splits (MTRY). The number of RF trees to grow was 500, and the number of predictor variables performing the data partitioning at each node was set to the MTRY value with the lowest out-of-bag error. The RF training models were validated with the validation dataset.

For LMR, as with the RF model creation procedure, we implemented this method twice, in the first iteration only ITC size metrics were used (13), whilst the second used a combination of ITC size and CI metrics (30) as predictor variables in the training dataset. We used a 10-fold cross-validation control and allowed a maximum

of six predictors in the final model. For all models, we verified relationship linearity, observation independence, constant variance and normal residual distribution. We used variance inflation factor (VIF) to evaluate models with more than one predictor for multicollinearity. Any predictor in a model with a VIF greater than four was removed, and the model was re-run. The linear regression models were validated with the validation dataset.

The predicted values from the RF and LMR models were evaluated by calculating the adjusted coefficient of determination (adjusted R^2), absolute and normalized root mean square error (RMSE and NRMSE, respectively), and absolute and normalized bias (Bias and NBias, respectively) based on the linear relationship between observed and predicted values using the independent validation datasets (summarized in Table S.1). We defined acceptable model accuracy as an NRMSE and NBias of <15% based upon the recommendation from Silva et al. (2017; 2018) for industrial loblolly pine sites. We used a two-sided Kolmogorov–Smirnov (KS) test and a Welch's t-test in R (R Core Team 2021) to compare the field- and DLS ITC-based DBH and stem volume estimates. A *p*-value of 0.05 or below was determined as significant. The empirical cumulative distribution function (ECDF) was calculated for the RF and LMR models of DBH and stem volume to compare distributions across the range of measurements. We also compared the ITC derived metrics of total tree height, HTLC, and crown horizontal size with their equivalent field values using equations 7–11 in Table S.1.

3. Results

3.1. Individual tree delineation accuracy

Field mortality (field recorded dead) of trees ranged from 3% of the total population in the NE to 15% at BL (Table 2). The overall survival rate was above 84% for all sites. The mean field total tree height ranged from 10 m at RH in 2017 to 16.5 m in the NE. Any field recorded stems with a total height below 4.7 m were considered as understory and removed.

Overall, our ITC delineation algorithm detected ≥80% of stems across all sites (Table 3). The greatest detection rate was recorded for the RH dataset in 2017, where 91% of trees were identified overall across all stem densities. ITC delineation accuracy varied with stem density (TPH) where more trees were missed at higher density. At 618 trees ha^{-1} our method missed 1–3% but at 1,853 trees ha^{-1} it missed 21–38%. We found the highest omission error at BL and the lowest commission error for the NE and RH in 2017 (Table 4).

3.2. Individual tree metrics

We considered our ITC-derived total tree height and HTLC estimates acceptable because their NRMSE and NBias were less than 15%. ITC-derived crown area estimates were just above our acceptable threshold, where NRMSE was less than 16%. ITC total height estimates were generally slightly (0.3 m) biased upwards from field measurements (i.e. 'Bias'; Table 5). HTLC estimate uncertainty and ITC estimates were greater than field measurements. ITC crown area estimates typically underestimated field measurements.

Table 3. Omission error for the Nelder (NE), Bladen Lakes (BL) and Reynolds Homestead (RH) sites among years and planting densities where individual tree crowns were delineated using drone laser scanning data.

Site	Total no. of alive trees	Initial trees per hectare	No. of trees missed	Proportion of total missed alive (%)
NE 2017	*839*	*All plots*	*135*	*16.09*
RH 2017	*9954*	*All plots*	*975*	*9.80*
	3296	618	52	1.58
	3331	1236	222	6.66
	3327	1853	701	21.07
BL 2017	*5780*	*All plots*	*1143*	*19.77*
	1913	618	54	2.88
	1934	1236	346	17.89
	1933	1853	743	38.39
RH 2021	*9774*	*All plots*	*1177*	*12.04*
	3249	618	42	1.32
	3284	1236	366	11.11
	3241	1853	771	23.73

Table 4. Commission error for the Nelder (NE), Bladen Lakes (BL) and Reynolds Homestead (RH) sites and years where individual tree crowns were delineated using drone laser scanning data.

Site	Additional delineations (number of trees)
NE 2017	16
RH 2017	46
BL 2017	112
RH 2021	135

3.3. Predictor variable selection

3.3.1. Models including tree size metrics only

All 17 ITC variables were considered important for both DBH and stem volume predictor variable selection. Model tuning for DBH determined the optimal MTRY value was 2 (OOBError = 1.82). Model tuning for stem volume determined the optimal MTRY value was 2 (OOBError = 6.89). The six most important RF model predictors ranked by importance (percentage increase in mean squared error) for both metrics are summarized in Table S.2. The predictors selected via the backward-stepwise LMR approach and assessment of VIF are summarized in Table S.3.

3.3.2. Models including tree size and competition index metrics

All 30 ITC variables were considered important for both DBH and stem volume predictor variable selection. Model tuning for DBH determined the optimal MTRY value was 2 (OOBError = 1.59). Model tuning for stem volume determined the optimal MTRY value was 2 (OOBError = 5.18). The six most important RF model predictors ranked by importance (percentage increase in mean squared error) for both metrics are summarized in Table S.4. Likewise, the predictors selected via the backward-stepwise LMR approach and the assessment of VIF are summarized in Table S.5.

Table 5. Individual tree metrics derived from DLS data collected from an unoccupied aerial vehicle compared to field measurements for the sites (Nelder (NE), Bladen Lakes (BL) and Reynolds Homestead (RH)) and years when measurements were completed. Normalized Bias (NBias) is noted in the Bias column.

Metric	Site	Adj. R^2	RMSE	NRMSE (%)	Bias
Total tree height (m)	*Overall*	*0.87*	*1.19*	*6.52*	*0.28 (1.53%)*
	NE 2017	0.67	0.98	9.10	0.33
	RH 2017	0.82	0.78	6.25	−0.12
	BL 2017	0.76	0.65	6.78	0.23
	RH 2021	0.70	0.92	8.44	0.31
Height to the live crown (m)	*Overall*	*0.74*	*1.54*	*12.44*	*0.73 (5.95%)*
	NE 2017	0.60	1.67	13.65	1.28
	RH 2017	0.53	1.39	11.85	0.85
	BL 2017	0.42	1.28	12.16	0.86
	RH 2021	0.50	1.98	14.24	0.75
Crown area (m^2)	*Overall*	*0.33*	*4.81*	*15.65*	*-0.40 (−1.36%)*
	NE 2017	0.52	5.04	14.91	−1.65
	RH 2017	0.27	4.07	14.90	−0.79
	BL 2017	0.27	4.87	14.64	1.23
	RH 2021	0.31	5.68	14.20	−1.26

3.4. Model validation

3.4.1. Models including tree size metrics only

We evaluated predictions against the validation dataset for models generated using individual tree size metrics only. The LMR models had a slightly greater adjusted R^2 and a slightly lower RMSE than the RF models (Table 6). Bias values were all low (NBias <0.2%) implying all of the models were unbiased. The predictions are illustrated in Figure S.3 (A for RF and B for LMR), where more uncertainty is evident at the extremes of DBH range (<10 or >30 cm).

The values given in Table 6, suggest there was a difference in correlation between RF and LMR when predicting individual tree stem volume. Stem volume distribution was evenly distributed for stems <0.3 m^3, but uncertainty increases for larger volumes (Figure S.3). Predicted RF model stem volumes for these stems were distributed evenly around the 1:1 line. This was true for the LMR predictions only when stem volume was below 0.2 m^3, increased uncertainty is evident for large stem sizes.

3.4.2. Models including tree size and competition index metrics

All models created using tree size and CI metrics produced higher levels of accuracy in terms of higher adjusted R^2 and lower RMSE values. When evaluated against the

Table 6. Individual tree metrics (stem diameter (DBH) and volume) derived from drone laser scanning data and estimated using the Random Forest model (RF) or linear multiple regression (LMR) compared to validation data for models including tree size metrics only.

Metric	Adj. R^2	RMSE	NRMSE (%)	Bias	NBias (%)
DBH RF (cm)	0.51	3.96	10.28	−0.07	−0.17
DBH LMR(cm)	0.56	3.79	9.83	−0.07	−0.19
Stem volume RF (m^3)	0.66	0.08	8.73	0.00	0.03
Stem volume LMR (m^3)	0.59	0.09	9.14	0.00	0.09

Table 7. Individual tree metrics (diameter (DBH) and volume) derived from drone laser scanning data and estimated using the Random Forest model (RF) or linear multiple regression (LMR) compared to validation data for models including tree size and competition index metrics.

Metric	Adj. R^2	RMSE	NRMSE (%)	Bias	NBias (%)
DBH RF (cm)	0.64	3.05	7.95	−0.09	−0.23
DBH LMR(cm)	0.62	3.13	8.17	−0.06	−0.22
Stem volume RF (m^3)	0.77	0.06	6.70	0.00	−0.01
Stem volume LMR (m^3)	0.70	0.07	7.58	0.00	0.03

validation dataset, the RF models had a slightly greater adjusted R^2 and a slightly lower RMSE than the LMR models (Table 7). RF and LMR models slightly overestimated the field measured DBH (0.06 to 0.09 cm bias) (Table 7), particularly for DBH values less than 12 cm (Figure 6a for RF, Figure 6b for LMR).

Stem volume distribution was uneven where most stems were <0.3 m^3 (Figure 6c for RF, Figure 6d for LMR). Predicted RF model stem volumes for these stems were distributed evenly around the 1:1 line. For the LMR model, the uncertainty increased for stems >0.3 m^3. The LMR model exhibited non-linearity between 0.0 and 0.2 m^3.

The RF and LMR stem volume and LMR DBH models were not significantly different from field measurements based on the Welch's paired t-test implying that the two populations had similar means (Table S.6). All KS tests were significant, indicating that the predicted and measured datasets do not have the same distribution.

DBH ECDF distributions for RF and LMR models deviated from observed values at the distribution extremes (Figure S.4A and S.4B, respectively). Predicted values exceeded observed at high DBH values and underestimated DBH at lower values. The stem volume RF model ECDF distribution followed the same patterns (Figure S.4C). The stem volume LMR model ECDF distribution was inconsistent in that the predicted distribution fell above and below the observed data throughout the distribution (Figure S.4D).

4. Discussion

4.1. Delineation of individual tree crowns

Our method to delineate ITCs from DLS derived VO_{index} and CHM raster and marker-based segmentation correctly located 61% to 99% of field-measured trees, depending on stem planting density. Our commission errors were generally low; however, sites with large total tree height variance had more commission error. Omission and commission error with ITC delineation are common, and our results compared favourably with a range of ITC delineation methods including raster and point-cloud segmentation with reported detection rates from 25% to 119% of codominant canopy trees (Kaartinen et al. 2012; Yao, Krzystek, and Heurich 2012; Silva et al. 2016; Wan Mohd Jaafar et al. 2018). Our VO_{index} was inspired by (Lee and Lucas 2007) work with HSCOI, and they reported accuracies of R^2 = 0.82, with an RMSE = 133 stems ha^{-1} at the plot scale.

Planting density (TPH) influenced ITC delineation where high planting density resulted in lower accuracy. For example, at 1,853 trees ha^{-1}, 61% to 79% of stems were correctly located, whereas at 618 trees ha^{-1} 97% to 99% were correctly located across our study sites. As stated in Krůček et al. (2020), errors of omission were more common for smaller trees than larger ones. We must assume that smaller tree crowns, particularly when

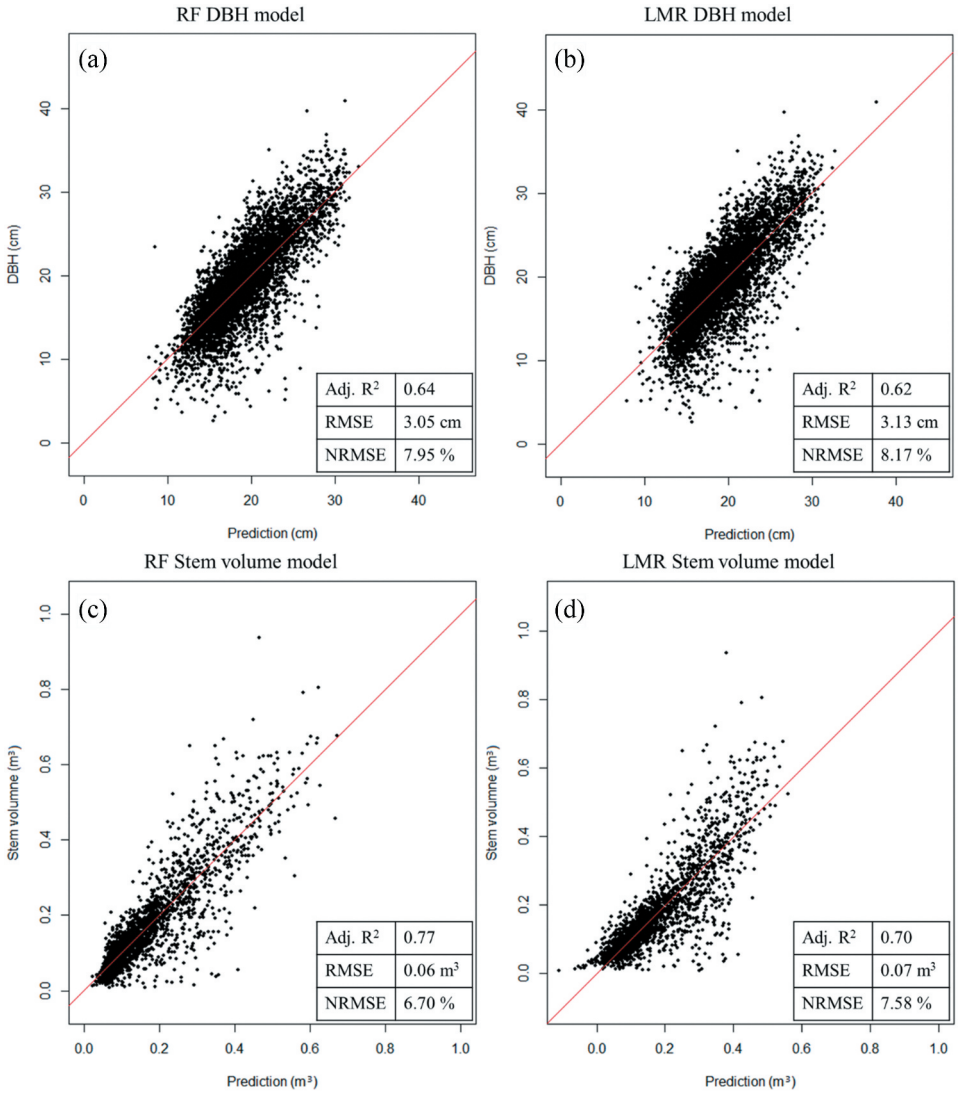

Figure 6. Models derived from ITC competition index and tree size metrics. DBH predicted using the Random Forest (RF) method for the validation dataset (a). DBH volume predicted using the LMR method for the validation dataset (b). Stem volume predicted using the RF method for the validation dataset (c). Stem volume predicted using the LMR method for the validation dataset (d). The red-line denotes the potential 1-to-1 line.

planted in high density in the current context, are often indistinguishable from their neighbours (Zhen, Quackenbush, and Zhang 2016). This implies that changes in acquisition types or delineation methods would be required under high stem densities to improve accuracy. While the omission error for large crowns was relatively small, here we assume omission was likely related to irregular crown DLS return density or over-topping (potentially caused by ramicorn branching in loblolly pine genotypes, e.g. Xiong et al. 2014) where an ITC class would represent a cluster of trees. Similarly, ITC delineation was less accurate at BL likely due to greater height variation resulting in a more variable

canopy structure compared to our other sites (see Table 2). Kaartinen et al. (2012) noted that ITC delineation methods were sensitive to forest canopy structural complexity where there was a reduced likelihood of correctly locating a short tree next to a tall neighbour. All other metrics (total tree height, HTLC, horizontal crown diameter, DBH and stem volume) were dependent on accurate ITC delineation, so errors for these variables will be greater with high density and variable canopies. Stand density and canopy variability may be better managed by segmenting the point-cloud, and given our high pulse-density datasets, future modifications to our ITC delineation approach may be warranted. An alternative approach, proposed by Yao, Krzystek, and Heurich (2012), is to segment the ALS point-cloud using a modification of a normalized cut segmentation to classify heterogeneous canopies into ITCs which may improve ITC delineation.

4.2. Individual tree crown metrics

Our ITC total height RMSE results were similar to the greatest accuracies reported (Table 8) in the literature. Sumnall et al. (2022) found that ITC total height RMSE decreased as pulse density increased. We used high pulse densities (>300 pulses m^{-2}) and overestimated height for RH and NE 2017 by 0.23 to 0.33 m but underestimated them at BL by 0.12 m. Assuming there was no field measurement error, this discrepancy may be caused by incorrectly estimated ground heights. The BL site was bedded, whereas the RH and NE sites were not. The beds were generally about 30–40 cm high, and these local differences in elevation may not have been accounted for correctly in ground classification. Differences in the time of data collection, particularly for RH 2021, may also account for some errors.

Our approach for estimating ITC HTLC from DLS (Adj. R^2 0.74, RMSE 1.54 m) compared well with other research (Table 8). Our HTLC bias was 0.73 m, implying an overestimation. Several potential explanations for this exist. First, our method was not sophisticated enough to discriminate among variable point densities, variably located foliage clusters, and noise encountered beneath the canopy where understory or crown components could not be reasonably classified within the point-cloud. Another explanation is that the number of returns from the lower canopy was not sufficient to describe lower canopy features, implying that the features we were estimating were not well represented even with high pulse densities. Finally, our HTLC field protocol entails measuring the height where the lowest live branch meets the main stem, which was different from our HTLC estimation method. Our HTLC estimation method identified the foliage associated with the lowest live branch or the bottom of the crown. Arguably, our HTLC method gives the height above which most of the foliage was found.

Our crown area estimates (Adj. R^2 0.33 and RMSE 4.81 m^2) compared poorly with previous studies that had an approximate (after converting to the area of a circle) RMSE of 1.18 to 3.39 m^2 (Table 8). Except for BL, we generally underestimated the crown area. With reference to Sumnall et al. (2022), we assume that the error was associated with the planting density. At the same time, crown area and closure varied with the relative effect of the management treatments, exhibiting differences in crown structural characteristics (as in Yáñez, Seiler, and Fox 2017). These factors may influence ITC delineation as crowns may be obscured by overlap with neighbouring crowns. This result implies that our approach based on segmenting features from a CHM may be insufficient to characterize

Table 8. Statistics (root mean square error (RMSE), coefficient of determination (R^2) and correlation coefficient (r)) from the literature where individual tree crown (ITC) metrics (total height, height to live crown (HTLC) and horizontal crown area) were estimated using LiDAR data from an airborne (ALS) or drone (DLS) laser scanner.

Metric	Overall accuracy	References
ALS ITC total height (m)	• RMSE 1.19 m (R^2 0.87);	This study;
	• RMSE 1.1 m (R^2 0.78 to 0.86);	(Kwak et al. 2007);
	• RMSE 1.3 m;	(Vastaranta et al. 2014);
	• RMSE 2.64 to 2.81 m (r 0.87);	(Falkowski et al. 2006);
	• RMSE 1.85 m (R^2 0.81);	(Lee and Lucas 2007);
	• RMSE 4.15 to 4.27 (R^2 0.93 to 0.96);	(Jakubowski et al. 2013);
DLS ITC total height (m)	• RMSE 1.19 (R^2 0.89);	This study;
	• RMSE 1.51 m (r 0.91);	(Corte et al. 2020a);
	• RMSE 1.44 m (R^2 0.86);	(Gyawali et al. 2022);
ITC HTLC (m)	• RMSE 1.54 to 1.62 m (R^2 0.72–0.92);	(Kato et al. 2009);
(low point density 4–20 points m^{-2})	• RMSE 1.62 m (R^2 0.88);	(Luo et al. 2018);
	• RMSE 1.25 m (R^2 0.4);	(Chamberlain, Meador, and Thode 2021);
ITC HTLC (m)	• RMSE 1.54 m (R^2 0.74);	This study;
(high point density 150–535 m^{-2})	• RMSE 3.55 to 3.66 m (R^2 0.20 to 0.31);	(Arkin et al. 2021); (Liu et al. 2021);
	• RMSE 1.13 m (R^2 0.98);	
ITC crown diameter (m)	• RMSE *2.47 m (R^2 0.33);	This study;
	• RMSE 1.29 to 2.02 m (r 0.2 to 0.85);	(Falkowski et al. 2008);
	• RMSE 1.68 m (R^2 0.57);	(Popescu and Zhao 2008);
	• RMSE 1.23 m (R^2 0.87);	(Ferraz et al. 2016);
	• RMSE 1.4 m (R^2 0.84 to 0.86);	(Wan Mohd Jaafar et al. 2018).

*Circle area converted to diameter.

crown area given the complex 3D nature of tree crowns (Silva et al. 2016). Finally, field measurements capturing crown diameter in two directions may not correspond to crown area estimates calculated as an ellipse.

4.3. Statistical estimates of stem diameter at breast height and volume

For all models, the inclusion of CI metrics improved the estimation accuracy, where R^2 values increased by 0.05 to 0.13 and NRMSE values decreased by 1.6% to 2.3%. The remainder of this section will discuss only those models that included CI metrics. The RF and LMR DBH models shared four predictor variables: (i) the CI calculated for ITC crown area; (ii) the CI calculated for ITC total tree height; (iii) horizontal crown volume for the top 50% of total height; and (iv) ITC total height. Not surprisingly, then, the RF and LMR models produced very similar results in terms of adj. R^2, RMSE and bias with the validation dataset (Table 7). CIs derived from field data enhanced stem DBH and volume predictive estimates (e.g. Pretzsch, Biber, and Ďurský 2002; Mailly, Turbis, and Pothier 2003; von Oheimb et al. 2011), it would appear that our ITC-derived metrics also improve estimation accuracy. Previous estimates of tree DBH have used ITC metrics as inputs to predictive models (e.g. Popescu 2007) and used ALS covariates summarizing the distribution of returns within the footprint of that delineated crown as predictor variables (Dalponte, Bruzzone, and Gianelle 2011). Yao, Krzystek, and Heurich (2012) and Wu et al. (2015) employed ITC metrics derived from the delineated tree 3D extent similar to our metrics and reported comparable RMSEs to our study.

Our estimates of individual tree DBH accuracy were, overall, unbiased and compared favourably to those found in the surrounding literature (see Table 9). Our field measured DBH ranged from 5 to 35 cm, which was considerably less than other studies (Yao et al., 2012, ~10–70 cm; and Wu et al., 2015, ~10–70 cm). We observed our largest deviations (between predicted and observed) from the validation samples at the distribution extremes where the training samples were sparse (Figure S.4). An increase in DBH range would likely improve model fit (da Silva and Seixas, 2017) and improve RF model utility, which cannot extrapolate beyond the training range. Similarly, sparse training samples may cause model underperformance (Coulston et al., 2016). Furthermore, the inclusion of a larger DBH range in our analysis would allow exploration of the non-linear trends observed in the LMR model.

Our RF and LMR stem volume models produced similar results although the LMR method exhibited non-linearity for small stem volumes. Both included CI metrics and shared two predictors (i) ITC total height and (ii) canopy volume for the top 50% of total height. We had few stem volumes >0.6 m^3 which may limit model predictive capabilities. Similar to our results, Chen et al. (2007) and Rubilar et al. (2008) found that the basal area was exponentially related to crown geometric volume and the stem volume was proportional to this. A summary of predictive accuracy examples within the surrounding literature is presented in Table 9, where our results compare favourably, and generally have a lower RMSE. Other studies have used ALS ITC total height (Silva et al. 2017; Corte et al. 2020b), ITC 3D crown volume, total tree height, and horizontal crown area metrics (Yao, Krzystek, and Heurich 2012; and Wu et al., 2015) and machine learning techniques (Corte et al. 2020b) to estimate individual tree stem volume. These studies had a much larger range of stem volume (up to 6 m^3) and generally reported higher R^2 and RMSE values. Table 9 summarizes values for both homogenous plantation forest and (semi-)natural forest ecosystems, in particular for the latter, Yao, Krzystek, and Heurich (2012) and Wu et al. (2015) include summaries of models generated for both coniferous and deciduous species. While there is no doubt a need for some

Table 9. Statistics (root mean square error (RMSE), normalized RMSE (NRMSE), mean average error (MAE) and coefficient of determination (R^2)) from the literature where individual tree crown (ITC) metrics (diameter at breast height (DBH) or stem volume) were estimated using LiDAR data from an airborne (ALS) or drone (DLS) laser scanner.

Metric	Overall accuracy	References
DBH	• RMSE 3.05–3.13 cm (R^2 0.62–0.64);	This study;
	• RMSE 8.7 cm (R^2 0.84);	(Lo and Lin 2012);
	• RMSE 4.08 to 4.58 cm (R^2 0.3);	(Corrao, Sparks, and Smith 2022);
	• RMSE 2.96–6.52 cm (R^2 0.66–0.95);	(Wu et al. 2015);
	• RMSE 4.15–5.33 cm (R^2 0.65–0.88);	(Yao, Krzystek, and Heurich 2012);
	• RMSE 3.73–4.16 cm (R^2 0.28–0.41)	(Corte et al. 2020b);
Stem volume	• RMSE 0.06–0.07 m^3 (R^2 0.7–0.77)	This study;
	• RMSE 0.91 m^3 (R^2 0.9);	(Lo and Lin 2012);
	• RMSE 0.15 m^3 (R^2 0.4);	(Corrao, Sparks, and Smith 2022);
	• MAE 0.59–0.65 m^3 (R^2 0.67–0.73);	(Dalponte, Bruzzone, and Gianelle 2011);
	• RMSE 0.31–0.75 m^3 (R^2 0.62–0.96);	(Wu et al. 2015);
	• RMSE 0.43–0.6 m^3 (R^2 0.66–0.91);	(Yao, Krzystek, and Heurich 2012);
	• NRMSE 8.48–10.13% (R^2 0.97–0.98);	(Silva et al. 2017);
	• RMSE 0.14–0.15 m^3 (R^2 0.43–0.5)	(Corte et al. 2020b);

degree of species specificity, individual tree crown metrics, similar to those used in this research, can be used in various contexts. The use of ITC derived CIs may be of potential benefit in these contexts as well.

4.4. Considerations and future work

Our results demonstrated the utility of including ITC dimensions and CI to improve estimates of tree DBH and individual tree stem volume. The continuous spatial coverage of DLS remote sensing data allowed us to identify neighbours automatically in 3D space to a greater degree than a typical field survey. However, more complicated canopy structures, like suppressed trees, may be missed with our method using a CHM to determine the horizontal extent. Yao, Krzystek, and Heurich (2012) proposed a method to segment the point-cloud directly to classify suppressed and understory coniferous or deciduous trees, a capability likely needed for operational forests. Non-homogeneous species forest contexts complicate the application of these approaches; Moe et al. (2020), however, demonstrated a fusion of UAV colour-imagery and ALS derived metrics to classify ITCs in mixed forest sites and model DBH for specific species. With improvements in DLS equipment, sufficient pulse densities and large-scan angle ranges have allowed the classification of specific tree features, such as the tree stem (Yao, Krzystek, and Heurich 2012; Neuville, Bates, and Jonard 2021). This implies that metrics from these features could be included in the future modelling in addition to the potential for direct measurements.

Our ability to delineate ITC objects was influenced by stem density and crown size (Sumnall et al. 2022). Our relatively small plots, homogeneous genotypes, and spatial arrangements differ from operational forests although our site conditions covered a wide range of silvicultural treatments prior to thinning, and our methods should be relatively robust in similar conditions. Kaartinen et al. (2012) and Zhen et al. (2016) demonstrated that the effectiveness of different ITC methods was dependent on the applied context. When used with different management conditions or context, our method's effectiveness is unknown.

The different genotypes existing in the current research context have different crown architectures. The degree to which neighbouring tree crowns overlap can have a marked impact on tree survival and growth (Zambrano et al. 2019). The degree to which individual tree crowns vertically overlap, or interlock, was not considered in the current research. As such, the competition of neighbour trees may not be completely accounted for. Future work could therefore attempt to estimate these attributes and evaluate their importance.

Within the context of the current study, we assumed that the metrics produced from two sensor systems were correct and analogous. Previous research has explored the issue of differences in acquisition parameters on prediction accuracy (e.g. Hopkinson 2006; Næsset 2009). Acquisition-specific considerations may be a source of uncertainty, given our differences in total height estimation between sites. Acquisitions using DLS and ALS vary in terms of sensor, altitude, laser power and footprint that may influence a system's ability to resolve a return (Goodwin, Coops, and Culvenor 2006; Shao et al. 2019; Marino et al. 2022). Different sensors can also have different canopy penetration capabilities, even when applied at the same location

(Kamoske et al. 2019; Yu et al. 2020). The use of different processing methods can also lead to differences in predictions (e.g. Van Leeuwen and Nieuwenhuis 2010). We used ground-based measurements as our reference. We did not address any errors associated with those measurements. Likewise, the collection of data at different times – for example, the difference in field data and DLS acquisition times for RH 2021 – is a likely source of uncertainty.

With high pulse densities available from ALS or DLS, the identification of individual stems directly from the point-cloud is possible (Mongus and Žalik 2015; Neuville, Bates, and Jonard 2021). Returns from 1.3 m above ground (typical DBH measurement height) are sparse and are dependent upon laser penetration to these features, implying that dense canopy occlusion would hinder these methods. Estimating these features directly would benefit forest management. Work to evaluate the inclusion of partial stem metrics – for example, if return density further up the stem could be consistently achieved – would improve individual tree size estimates. Lamb et al. (2018) demonstrated the use of ALS derived inventory metrics as inputs to conventional growth models, which illustrates the potential of such datasets for prediction.

5. Conclusions

In conclusion, DLS (and ALS) data have great potential to monitor forests because of their ability to characterize individual tree parameters. We presented a novel method to identify ITCs and their neighbours and extract dimensional metrics (total tree height, HTLC, horizontal crown area, DBH and stem volume) in managed loblolly pine stands with variable planting densities and crown architectures. Our results provide evidence that the inclusion of ITC size and CI improves stem-size estimation accuracy, noticeably when compared to models using tree size metrics alone. The neighbourhood CI metrics can be computed from any ITC metric and are likely compatible with ALS data acquired over plantation pine forest. Future research is warranted in further developing these approaches for other environmental context and ALS datasets. Due to the success of these ITC metrics, airborne remote sensing's ability to provide accurate, and near-complete, inventories of a forest area holds a great deal of potential in terms of forest management and planning

5.1. Research highlights

- We delineated individual trees from three unoccupied aerial vehicle laser scanner datasets;
- We developed a new method to assess the competitive neighbourhood around each tree;
- Our models provide LiDAR-derived estimates of individual tree stem diameter and volume;
- A combination of tree crown size and competition metrics provided the best predictions of stem diameter and volume;
- Random Forest predictions only slightly outperform those from linear regression.

Acknowledgements

This work was primarily funded by the Forest Productivity Cooperative. This work was also supported by the Virginia Agricultural Experiment Station (Critz, Virginia), and the USDA National Institute of Food and Agriculture, U.S. Department of Agriculture (Washington, DC, USA).

Disclosure statement

No potential conflict of interest was reported by the authors.

ORCID

Rachel L. Cook http://orcid.org/0000-0001-7309-3971

Data availability statement

The data that support the findings of this study are available from the corresponding author, MJS, upon reasonable request.

References

Alig, R. J., and B. J. Butler. 2004. *Area Changes for Forest Cover Types in the United States, 1952 to 1997, with Projections to 2050*. USDA Forest Service Gen. Tech. Rep. PNW-GTR-613, Vol. 613, 106. Portland, OR: Pacific Northwest Research Station.

Arkin, J., N. C. Coops, L. D. Daniels, and A. Plowright. 2021. "Estimation of Vertical Fuel Layers in Tree Crowns Using High Density LiDar Data." *Remote Sensing* 13 (22): 4598. doi:10.3390/rs13224598.

Avery, T. E., and H. E. Burkhart. 2001. *Forest Measurements*. 5th ed. Boston, MA: McGraw-Hill.

Barrett, F., R. E. McRoberts, E. Tomppo, E. Cienciala, and L. T. Waser. 2016. "A Questionnaire-Based Review of the Operational Use of Remotely Sensed Data by National Forest Inventories." *Remote Sensing of Environment* 174: 279–289. doi:10.1016/j.rse.2015.08.029.

Bechtold, W. A., and K. C. Randolph, 2018. FIA Crown Analysis Guide. (Accessed 29 November 2022). Available at: https://www.fs.usda.gov/srsfia/crowns/Crown%20Analysis%20Guide%20v2.pdf

Bella, I. E. 1971. "A New Competition Model for Individual Trees." *Forest science* 17 (3): 364–372.

Biging, G. S., and M. Dobbertin. 1992. "A Comparison of Distance-Dependent Competition Measures for Height and Basal Area Growth of Individual Conifer Trees." *Forest science* 38 (3): 695–720.

Bivand, R., T. Keitt, and B. Rowlingson 2021. Rgdal: Bindings for the 'Geospatial' Data Abstraction Library. R Package Version 1.5-28. https://CRAN.R-project.org/package=rgdal

Bivand, R., and N. Lewin-Koh 2022. Maptools: Tools for Handling Spatial Objects. R Package Version 1.1-3. https://CRAN.R-project.org/package=maptools

Bivand, R. S., E. Pebesma, and V. Gomez-Rubio. 2013. *Applied Spatial Data Analysis with R*. Second edition ed. Springer, NY. https://asdar-book.org/.

Bivand, R., and C. Rundel 2021. Rgeos: Interface to Geometry Engine – Open Source ('GEOS'). R Package Version 0.5-9. https://CRAN.R-project.org/package=rgeos

Breiman, L. 2001. "Random Forests." *Machine Learning* 45 (1): 5–32. Oct, 2001. doi:10.1023/A:1010933404324.

Burkhart, H. E., and M. Tomé. 2012. *Modeling Forest Trees and Stands*. Dordrecht: Springer Science & Business Media.

Carter, D. R., T. J. Albaugh, O. C. Campoe, J. J. Grossman, R. A. Rubilar, M. Sumnall, C. A. Maier, R. L. Cook, and T. R. Fox. 2020. "Complementarity Increases Production in Genetic Mixture of Loblolly Pine (*Pinus taeda* L.) Throughout Planted Range." *Ecosphere* 11 (11): e03279. doi:10.1002/ecs2.3279.

Castagneri, D., G. Vacchiano, E. Lingua, and R. Motta. 2008. "Analysis of Intraspecific Competition in Two Subalpine Norway Spruce (*Picea abies* (L.) Karst.) Stands in Paneveggio (Trento, Italy)." *Forest Ecology and Management* 255 (3–4): 651–659. doi:10.1016/j.foreco.2007.09.041.

Chamberlain, C. P., A. J. S. Meador, and A. E. Thode. 2021. "Airborne Lidar Provides Reliable Estimates of Canopy Base Height and Canopy Bulk Density in Southwestern Ponderosa Pine Forests." *Forest Ecology and Management* 481: 118695. doi:10.1016/j.foreco.2020.118695.

Chen, Q., P. Gong, D. Baldocchi, and Y. Q. Tian. 2007. "Estimating Basal Area and Stem Volume for Individual Trees from Lidar Data." *Photogrammetric Engineering & Remote Sensing* 73 (12): 1355–1365. doi:10.14358/PERS.73.12.1355.

Chen, G., and G. J. Hay. 2011. "A Support Vector Regression Approach to Estimate Forest Biophysical Parameters at the Object Level Using Airborne Lidar Transects and Quickbird Data." *Photogrammetric Engineering & Remote Sensing* 77 (7): 733–741. doi:10.14358/PERS.77.7.733.

Corona, P. 2010. "Integration of Forest Mapping and Inventory to Support Forest Management." *iForest-Biogeosciences and Forestry* 3 (3): 59. doi:10.3832/ifor0531-003.

Corrao, M. V., A. M. Sparks, and A. M. Smith. 2022. "A Conventional Cruise and Felled-Tree Validation of Individual Tree Diameter, Height and Volume Derived from Airborne Laser Scanning Data of a Loblolly Pine (*P. taeda*) Stand in Eastern Texas." *Remote Sensing* 14 (11): 2567. doi:10.3390/rs14112567.

Corte, D. A. P., F. E. Rex, D. R. A. D. Almeida, C. R. Sanquetta, C. A. Silva, M. M. Moura, B. Wilkinson, et al. 2020a. "Measuring Individual Tree Diameter and Height Using GatorEye High-Density UAV-Lidar in an Integrated Crop-Livestock-Forest System." *Remote Sensing* 12 (5): 863. doi:10.3390/rs12050863.

Corte, D. A. P., D. V. Souza, F. E. Rex, C. R. Sanquetta, M. Mohan, C. A. Silva, A. M. A. Zambrano, et al. 2020b. "Forest Inventory with High-Density UAV-Lidar: Machine Learning Approaches for Predicting Individual Tree Attributes." *Computers and Electronics in Agriculture* 179: 105815. doi:10.1016/j.compag.2020.105815.

Costa, E. A., C. A. G. Finger, and A. F. Hess. 2018. "Competition Indices and Their Relationship with Basal Area Increment of Araucaria." *The Journal of Agricultural Science* 10 (5): 198–210. doi:10.5539/jas.v10n5p198.

Coulston, J. W., C. E. Blinn, V. A. Thomas, and R. H. Wynne. 2016. "Approximating Prediction Uncertainty for Random Forest Regression Models." *Photogrammetric Engineering & Remote Sensing* 82 (3): 189–197. doi:10.14358/PERS.82.3.189.

Dalponte, M., L. Bruzzone, and D. Gianelle. 2011. "A System for the Estimation of Single-Tree Stem Diameter and Volume Using Multireturn LiDar Data." *IEEE Transactions on Geoscience and Remote Sensing* 49 (7): 2479–2490. doi:10.1109/TGRS.2011.2107744.

da Silva, M. S., and T. M. Seixas. 2017. "The Role of Data Range in Linear Regression." *The Physics Teacher* 55 (6): 371–372. doi:10.1119/1.4999736.

Dean, T. J., Q. V. Cao, S. D. Roberts, and D. L. Evans. 2009. "Measuring Heights to Crown Base and Crown Median with LiDar in a Mature, Even-Aged Loblolly Pine Stand." *Forest Ecology and Management* 257 (1): 126–133. doi:10.1016/j.foreco.2008.08.024.

Dowle, M., and A. Srinivasan 2021. Data.Table: Extension of `data.Frame`. R Package Version 1.14.2. https://CRAN.R-project.org/package=data.table

Ellenberg, H. 1996. *Vegetation Mitteleuropas mit den Alpen*. 5 Auflage, 1096. Stuttgart: Verlag Eugen Ulmer.

Falkowski, M. J., A. M. Smith, P. E. Gessler, A. T. Hudak, L. A. Vierling, and J. S. Evans. 2008. "The Influence of Conifer Forest Canopy Cover on the Accuracy of Two Individual Tree Measurement Algorithms Using LiDar Data." *Canadian Journal of Remote Sensing* 34 (S2): S338–350. doi:10.5589/m08-055.

Falkowski, M. J., A. M. Smith, A. T. Hudak, P. E. Gessler, L. A. Vierling, and N. L. Crookston. 2006. "Automated Estimation of Individual Conifer Tree Height and Crown Diameter via Two-Dimensional Spatial Wavelet Analysis of LiDar Data." *Canadian Journal of Remote Sensing* 32 (2): 153–161. doi:10.5589/m06-005.

Ferraz, A., S. Saatchi, C. Mallet, and V. Meyer. 2016. "Lidar Detection of Individual Tree Size in Tropical Forests." *Remote Sensing of Environment* 183: 318–333. doi:10.1016/j.rse.2016.05.028.

Fox, T. R., E. J. Jokela, and H. L. Allen. 2007. "The Development of Pine Plantation Silviculture in the Southern United States." *Journal of Forestry* 105 (7): 337–347.

Fridman, J., S. Holm, M. Nilsson, P. Nilsson, A. H. Ringvall, and G. Ståhl. 2014. "Adapting National Forest Inventories to Changing Requirements – The Case of the Swedish National Forest Inventory at the Turn of the 20th Century." *Silva Fennica* 48 (3). doi:10.14214/sf.1095.

Goodwin, N. R., N. C. Coops, and D. S. Culvenor. 2006. "Assessment of Forest Structure with Airborne LiDar and the Effects of Platform Altitude." *Remote sensing of environment* 103 (2): 140–152. doi:10.1016/j.rse.2006.03.003.

Gyawali, A., M. Aalto, J. Peuhkurinen, M. Villikka, and T. Ranta. 2022. "Comparison of Individual Tree Height Estimated from LiDar and Digital Aerial Photogrammetry in Young Forests." *Sustainability* 14 (7): 3720. doi:10.3390/su14073720.

Habel, K., R. Grasman, R. B. Gramacy, P. Mozharovskyi, and D. C. Sterratt 2019. Geometry: Mesh Generation and Surface Tessellation. R Package Version 0.4.5. https://CRAN.R-project.org/package=geometry

Hardin, P. J., V. Lulla, R. R. Jensen, and J. R. Jensen. 2019. "Small Unmanned Aerial Systems (Suas) for Environmental Remote Sensing: Challenges and Opportunities Revisited." *GIScience & Remote Sensing* 56 (2): 309–322. doi:10.1080/15481603.2018.1510088.

Hegyi, F. 1974. "A Simulation Model for Managing Jack-Pine Stands Simulation." *Royal Colloid For, Research Notes* 30: 74–90.

Hijmans, R. J. 2022. Raster: Geographic Data Analysis and Modeling. R Package Version 3.5-15. https://CRAN.R-project.org/package=raster

Hilker, T., M. A. Wulder, and N. C. Coops. 2008. "Update of Forest Inventory Data with Lidar and High Spatial Resolution Satellite Imagery." *Canadian Journal of Remote Sensing* 34 (1): 5–12. doi:10.5589/m08-004.

Holmgren, J., and Å. Persson. 2004. "Identifying Species of Individual Trees Using Airborne Laser Scanner." *Remote Sensing of Environment* 90 (4): 415–423. doi:10.1016/S0034-4257(03)00140-8.

Hopkinson, C., 2006. The Influence of Lidar Acquisition Settings on Canopy Penetration and Laser Pulse Return Characteristics. In *2006 IEEE International Symposium on Geoscience and Remote Sensing*, 2420–2423. Denver, CO, USA: IEEE.

Hyyppä, J, H. Hyyppä, X. Yu, H. Kaartinen, A. Kukko, and M. Holopainen. 2017. "Forest Inventory Using Small-Footprint Airborne Lidar Shan, Ji, Toth, Charles." In *Topographic Laser Ranging and Scanning: Principles and Processing*, 335–370. Boca Raton, FL, USA: CRC Press.

Jakubowski, M. K., W. Li, Q. Guo, and M. Kelly. 2013. "Delineating Individual Trees from LiDar Data: A Comparison of Vector-And Raster-Based Segmentation Approaches." *Remote Sensing* 5 (9): 4163–4186. doi:10.3390/rs5094163.

Jenkins, J. C., R. A. Birdsey, and Y. Pan. 2001. "Biomass and NPP Estimation for the Mid-Atlantic Region (USA) Using Plot-level Forest Inventory Data." *Ecological Applications* 11 (4): 1174–1193. doi:10.1890/1051-0761(2001)011[1174:BANEFT]2.0.CO;2.

Kaartinen, H., J. Hyyppa, X. W. Yu, M. Vastaranta, H. Hyyppa, A. Kukko, M. Holopainen, et al. 2012. "An International Comparison of Individual Tree Detection and Extraction Using Airborne Laser Scanning." *Remote Sensing* 4 (4): 950–974. doi:10.3390/rs4040950.

Kamoske, A. G., K. M. Dahlin, S. C. Stark, and S. P. Serbin. 2019. "Leaf Area Density from Airborne Lidar: Comparing Sensors and Resolutions in a Temperate Broadleaf Forest Ecosystem." *Forest Ecology and Management* 433: 364–375. doi:10.1016/j.foreco.2018.11.017.

Kangas, A., and M. Maltamo. 2006. In *Forest Inventory: Methodology and Applications*, edited by von Gadow Klaus, Pukkala Timo, Tomé Margarida. Vol. 10. Dordrecht, Netherlands : Springer.

Kato, A., L. M. Moskal, P. Schiess, M. E. Swanson, D. Calhoun, and W. Stuetzle. 2009. "Capturing Tree Crown Formation Through Implicit Surface Reconstruction Using Airborne Lidar Data." *Remote Sensing of Environment* 113 (6): 1148–1162. doi:10.1016/j.rse.2009.02.010.

Korhonen, L., J. Vauhkonen, A. Virolainen, A. Hovi, and I. Korpela. 2013. "Estimation of Tree Crown Volume from Airborne Lidar Data Using Computational Geometry." *International Journal of Remote Sensing* 34 (20): 7236–7248. doi:10.1080/01431161.2013.817715.

Krůček, M., K. Král, K. C. Cushman, A. Missarov, and J. R. Kellner. 2020. "Supervised Segmentation of Ultra-High-Density Drone Lidar for Large-Area Mapping of Individual Trees." *Remote Sensing* 12 (19): 3260. doi:10.3390/rs12193260.

Kuhn, M. 2021. Caret: Classification and Regression Training. R Package Version 6.0-90. https://CRAN.R-project.org/package=caret

Kursa, M. B., and W. R. Rudnicki. 2010. "Feature Selection with the Boruta Package." *Journal of Statistical Software* 36(11): 1–13. URL http://www.jstatsoft.org/v36/i11/10.18637/jss.v036.i11

Kwak, D. A., W. K. Lee, J. H. Lee, G. S. Biging, and P. Gong. 2007. "Detection of Individual Trees and Estimation of Tree Height Using LiDar Data." *Journal of Forest Research* 12 (6): 425–434. doi:10.1007/s10310-007-0041-9.

Lamb, S. M., D. A. MacLean, C. R. Hennigar, and D. G. Pitt. 2018. "Forecasting Forest Inventory Using Imputed Tree Lists for LiDar Grid Cells and a Tree-List Growth Model." *Forests* 9 (4): 167. doi:10.3390/f9040167.

Lee, A. C., and R. M. Lucas. 2007. "A LiDar-Derived Canopy Density Model for Tree Stem and Crown Mapping in Australian Forests." *Remote Sensing of Environment* 111 (4): 493–518. doi:10.1016/j.rse.2007.04.018.

Lin, Y., J. Hyyppä, and A. Jaakkola. 2011. "Mini-UAV-borne LIDAR for fine-scale mapping." *IEEE Geoscience and Remote Sensing Letters* 8: 426–430.

Liu, X., Y. Hao, F. R. A. Widagdo, L. Xie, L. Dong, and F. Li. 2021. "Predicting Height to Crown Base of Larix Olgensis in Northeast China Using UAV-LiDar Data and Nonlinear Mixed Effects Models." *Remote Sensing* 13 (9): 1834. doi:10.3390/rs13091834.

Lo, C. S., and C. Lin. 2012. "Growth-Competition-Based Stem Diameter and Volume Modeling for Tree-Level Forest Inventory Using Airborne LiDar Data." *IEEE Transactions on Geoscience and Remote Sensing* 51 (4): 2216–2226. doi:10.1109/TGRS.2012.2211023.

Luo, L., Q. Zhai, Y. Su, Q. Ma, M. Kelly, and Q. Guo. 2018. "Simple Method for Direct Crown Base Height Estimation of Individual Conifer Trees Using Airborne LiDar Data." *Optics Express* 26 (10): A562–578. doi:10.1364/OE.26.00A562.

Mailly, D., S. Turbis, and D. Pothier. 2003. "Predicting Basal Area Increment in a Spatially Explicit, Individual Tree Model: A Test of Competition Measures with Black Spruce." *Canadian Journal of Forest Research* 33 (3): 435–443. doi:10.1139/x02-122.

Marino, E., J. L. Tomé, C. Hernando, M. Guijarro, and J. Madrigal. 2022. "Transferability of Airborne LiDar Data for Canopy Fuel Mapping: Effect of Pulse Density and Model Formulation." *Fire* 5 (5): 126. doi:10.3390/fire5050126.

McKeand, S., T. Mullin, T. Byram, and T. White. 2003. "Deployment of Genetically Improved Loblolly and Slash Pines in the South." *Journal of Forestry* 101 (3): 32–37.

Messinger, M., G. P. Asner, and M. Silman. 2016. "Rapid Assessments of Amazon Forest Structure and Biomass Using Small Unmanned Aerial Systems." *Remote Sensing* 8 (8): 615. doi:10.3390/rs8080615.

Moe, K. T., T. Owari, N. Furuya, T. Hiroshima, and J. Morimoto. 2020. "Application of UAV Photogrammetry with LiDar Data to Facilitate the Estimation of Tree Locations and DBH Values for High-Value Timber Species in Northern Japanese Mixed-Wood Forests." *Remote Sensing* 12 (17): 2865. doi:10.3390/rs12172865.

Mongus, D., and B. Žalik. 2015. "An Efficient Approach to 3D Single Tree-Crown Delineation in LiDar Data." *Isprs Journal of Photogrammetry and Remote Sensing* 108: 219–233. doi:10.1016/j.isprsjprs.2015.08.004.

Næsset, E. 2009. "Effects of Different Sensors, Flying Altitudes, and Pulse Repetition Frequencies on Forest Canopy Metrics and Biophysical Stand Properties Derived from Small-Footprint Airborne Laser Data." *Remote Sensing of Environment* 113 (1): 148–159. doi:10.1016/j.rse.2008.09.001.

Næsset, E. 2014. "Area-Based Inventory in Norway – From Innovation to an Operational Reality." In *Forestry Applications of Airborne Laser Scanning,* edited byMaltamo Matti, Næsset Erik, Vauhkonen Jari, 215–240. Dordrecht: Springer.

Namkoong, G. 1965. Application of Nelder's Designs in Tree Improvement Research. In: *Southern Conference on Forest Tree Improvement, 8. Savannah. Proceedings*. *Macon*, *SCFTI*. p.24–37.

Nelder, J. A. 1962. "New Kinds of Systematic Designs for Spacing Experiments." *Biometrics* 18 (3): 283–307. doi:10.2307/2527473.

Neuville, R., J. S. Bates, and F. Jonard. 2021. "Estimating Forest Structure from UAV-Mounted LiDar Point Cloud Using Machine Learning." *Remote Sensing* 13 (3): 352. doi:10.3390/rs13030352.

Pebesma, E. 2018. "Simple Features for R: Standardized Support for Spatial Vector Data." *The R Journal* 10 (1): 439–446. doi:10.32614/RJ-2018-009.

Piekenbrock, H. M., and M. D. Doran. 2019. "Dbscan: Fast Density-Based Clustering with R." *Journal of Statistical Software* 91 (1): 1–30. doi:10.18637/jss.v091.i01.

Pond, N. C., R. E. Froese, and L. M. Nagel. 2014. "Sustainability of the Selection System in Northern Hardwood Forests." *Forest science* 60 (2): 374–381. doi:10.5849/forsci.12-113.

Popescu, S. C. 2007. "Estimating Biomass of Individual Pine Trees Using Airborne Lidar." *Biomass & bioenergy* 31 (9): 646–655. doi:10.1016/j.biombioe.2007.06.022.

Popescu, S. C., R. H. Wynne, and R. F. Nelson. 2003. "Measuring Individual Tree Crown Diameter with Lidar and Assessing Its Influence on Estimating Forest Volume and Biomass." *Canadian Journal of Remote Sensing* 29 (5): 564–577. doi:10.5589/m03-027.

Popescu, S. C., and K. Zhao. 2008. "A Voxel-Based LiDar Method for Estimating Crown Base Height for Deciduous and Pine Trees." *Remote Sensing of Environment, Vol* 112 (3): 767–781. doi:10.1016/j.rse.2007.06.011.

Premer, M. I., S. Chhin, and J. Zhang. 2021. "Local Testing and Calibration of Species-Specific Competition Indices in Sierran Mixed-Conifer Forests: Application Transfer to Evolving Objectives." *Canadian Journal of Forest Research* 51 (4): 524–532. doi:10.1139/cjfr-2020-0193.

Pretzsch, H., P. Biber, and J. Ďurský. 2002. "The Single Tree-Based Stand Simulator SILVA: Construction, Application and Evaluation." *Forest Ecology and Management* 162 (1): 3–21. doi:10.1016/S0378-1127(02)00047-6.

Radtke, P. J., J. A. Westfall, and H. E. Burkhart. 2003. "Conditioning a Distance-Dependent Competition Index to Indicate the Onset of Inter-Tree Competition." *Forest Ecology and Management* 175 (1–3): 17–30. doi:10.1016/S0378-1127(02)00118-4.

Randolph, K. C. 2015. *Benefits and Limitations of Using Standard Forest Inventory and Analysis Data to Describe the Extent of a Catastrophic Weather Event. Asheville, NC*. US Department of Agriculture Forest Service, Southern Research StationVol. 55 1–10. *e-Res. Pap. SRS-55*.

R Core Team. 2021. *R: A Language and Environment for Statistical Computing*. Vienna, Austria: R Foundation for Statistical Computing. URL https://www.R-project.org/.

Rothmund, S., N. Vouillamoz, and M. Joswig. 2017. "Mapping Slow-Moving Alpine Landslides by UAV—opportunities and Limitations." *The Leading Edge* 36 (7): 571–579. doi:10.1190/tle36070571.1.

Roussel, J. R., and D. Auty 2022. Airborne LiDar Data Manipulation and Visualization for Forestry Applications. R Package Version 4.0.0. https://cran.r-project.org/package=lidR

Roussel, J. -R., D. Auty, N. C. Coops, P. Tompalski, T. R. H. Goodbody, A. S. Meador, J. -F. Bourdon, F. de Boissieu, and A. Achim. 2020. "LidR: An R Package for Analysis of Airborne Laser Scanning (ALS) Data." *Remote Sensing of Environment* 251: 112061. doi:10.1016/j.rse.2020.112061.

Rubilar, R., L. Blevins, J. Toro, A. Vita, and F. Muñoz. 2008. "Early Response of Pinus Radiata Plantations to Weed Control and Fertilization on Metamorphic Soils of the Coastal Range, Maule Region, Chile." *Bosque (Valdivia)* 29 (1): 74–84. doi:10.4067/S0717-92002008000100009.

Scott, C. T., and J. H. Gove. 2002. *Forest Inventory Encyclopedia of Environmetrics*, 814–820. *Chichester*: Wiley.

Shao, G., S. C. Stark, D. R. de Almeida, and M. N. Smith. 2019. "Towards High Throughput Assessment of Canopy Dynamics: The Estimation of Leaf Area Structure in Amazonian Forests with Multitemporal Multi-Sensor Airborne Lidar." *Remote Sensing of Environment* 221: 1–13. doi:10.1016/j.rse.2018.10.035.

Silva, C. A., A. T. Hudak, L. A. Vierling, E. L. Loudermilk, J. J. O'Brien, J. K. Hiers, S. B. Jack, et al. 2016. "Imputation of Individual Longleaf Pine (Pinus Palustris Mill.) Tree Attributes from Field and LiDar Data." *Canadian Journal of Remote Sensing* 42 (5): 554–573. doi:10.1080/07038992.2016.1196582.

Silva, C. A., C. Klauberg, A. T. Hudak, L. A. Vierling, W. S. W. M. Jaafar, M. Mohan, M. Garcia, A. Ferraz, A. Cardil, and S. Saatchi. 2017. "Predicting Stem Total and Assortment Volumes in an Industrial *Pinus taeda* L. Forest Plantation Using Airborne Laser Scanning Data and Random Forest." *Forests* 8 (7): 254. doi:10.3390/f8070254.

Silva, C. A., C. Klauberg, A. T. Hudak, L. A. Vierling, V. Liesenberg, L. G. Bernett, C. F. Scheraiber, and E. R. Schoeninger. 2018. "Estimating Stand Height and Tree Density in *Pinus taeda* Plantations Using In-Situ Data, Airborne LiDar and K-Nearest Neighbor Imputation." *Anais da Academia Brasileira de Ciências* 90 (1): 295–309. doi:10.1590/0001-3765201820160071.

Silva, A. D., and R. P. Lima. 2017. "Determination of Maximum Curvature Point with the R Package Soilphysics." *International Journal of Current Research* 9 (1): 45241–45245.

Sumnall, M. J., T. J. Albaugh, D. R. Carter, R. L. Cook, W. C. Hession, O. C. Campoe, R. A. Rubilar, R. H. Wynne, and V. A. Thomas. 2022. "Effect of Varied Unmanned Aerial Vehicle Laser Scanning Pulse Density on Accurately Quantifying Forest Structure." *International Journal of Remote Sensing* 43 (2): 721–750. doi:10.1080/01431161.2021.2023229.

Sumnall, M., T. R. Fox, R. H. Wynne, and V. A. Thomas. 2017. "Mapping the Height and Spatial Cover of Features Beneath the Forest Canopy at Small-Scales Using Airborne Scanning Discrete Return Lidar." *Isprs Journal of Photogrammetry and Remote Sensing* 133: 186–200. doi:10.1016/j.isprsjprs.2017.10.002.

Sumnall, M., A. Peduzzi, T. R. Fox, R. H. Wynne, and V. A. Thomas. 2016. "Analysis of a Lidar Voxel-Derived Vertical Profile at the Plot and Individual Tree Scales for the Estimation of Forest Canopy Layer Characteristics." *International Journal of Remote Sensing* 37 (11): 2653–2681. doi:10.1080/01431161.2016.1183833.

Sumnall, M. J., A. Trlica, D. R. Carter, R. L. Cook, M. L. Schulte, O. C. Campoe, R. A. Rubilar, R. H. Wynne, and V. A. Thomas. 2021. "Estimating the Overstory and Understory Vertical Extents and Their Leaf Area Index in Intensively Managed Loblolly Pine (*Pinus taeda* L.) Plantations Using Airborne Laser Scanning." *Remote Sensing of Environment* 254: 112250. doi:10.1016/j.rse.2020.112250.

Tasissa, G., H. E. Burkhart, and R. L. Amateis. 1997. "Volume and Taper Equations for Thinned and Unthinned Loblolly Pine Trees in Cutover, Site-Prepared Plantations." *Southern Journal of Applied Forestry* 21 (3): 146–152. doi:10.1093/sjaf/21.3.146.

Tinkham, W. T., P. R. Mahoney, A. T. Hudak, G. M. Domke, M. J. Falkowski, C. W. Woodall, and A. M. Smith. 2018. "Applications of the United States Forest Inventory and Analysis Dataset: A Review and Future Directions." *Canadian Journal of Forest Research* 48 (11): 1251–1268. doi:10.1139/cjfr-2018-0196.

Torres-Sánchez, J., F. López-Granados, N. Serrano, O. Arquero, and J. M. Peña. 2015. "High-Throughput 3-D Monitoring of Agricultural-Tree Plantations with Unmanned Aerial Vehicle (UAV) Technology." *PLoS One* 10 (6): e0130479. doi:10.1371/journal.pone.0130479.

Turner, R. 2021. Deldir: Delaunay Triangulation and Dirichlet (Voronoi) Tessellation. R Package Version 1.0-6. https://CRAN.R-project.org/package=deldir

Van Leeuwen, M., and M. Nieuwenhuis. 2010. "Retrieval of Forest Structural Parameters Using LiDar Remote Sensing." *European Journal of Forest Research* 129 (4): 749–770. doi:10.1007/s10342-010-0381-4.

Vasilescu, M. M. 2013. "Standard Error of Tree Height Using Vertex III. Bulletin of the Transilvania University of Brasov." *Forestry, Wood Industry, Agricultural Food Engineering Series II* 6 (2): 75.

Vastaranta, M., N. Saarinen, V. Kankare, M. Holopainen, H. Kaartinen, J. Hyyppä, and H. Hyyppä. 2014. "Multisource Single-Tree Inventory in the Prediction of Tree Quality Variables and Logging Recoveries." *Remote Sensing* 6 (4): 3475–3491. doi:10.3390/rs6043475.

Vauhkonen, J., M. Maltamo, R. E. McRoberts, and E. Næsset. 2014. "Introduction to Forestry Applications of Airborne Laser Scanning." In *Forestry Applications of Airborne Laser Scanning,* edited byMaltamo Matti, Næsset Erik, Vauhkonen Jari, 1–16. Dordrecht: Springer.

Velodyn. 2019. "VLP-16 User Manual, Velodyn." Accessed 9 November 2021. https://velodynelidar.com/wp-content/uploads/2019/12/63-9243-Rev-E-VLP-16-User-Manual.pdf

Venables, W. N., and B. D. Ripley. 2002. *Modern Applied Statistics with S*. ISBN 0-387-95457-0. Fourth Edition ed. *New York*: Springer.

von Oheimb, G., A. C. Lang, H. Bruelheide, D. I. Forrester, I. Wäsche, M. Yu, and W. Härdtle. 2011. "Individual-Tree Radial Growth in a Subtropical Broad-Leaved Forest: The Role of Local Neighbourhood Competition." *Forest Ecology and Management* 261 (3): 499–507. doi:10.1016/j.foreco.2010.10.035.

Wan Mohd Jaafar, W. S., I. H. Woodhouse, C. A. Silva, H. Omar, K. N. Abdul Maulud, A. T. Hudak, C. Klauberg, A. Cardil, and M. Mohan. 2018. "Improving Individual Tree Crown Delineation and Attributes Estimation of Tropical Forests Using Airborne LiDar Data." *Forests* 9 (12): 759. doi:10.3390/f9120759.

Wear, D. N., and J. G. Greis. 2002. *Southern Forest Resource Assessment*. Vol. 53. Asheville, NC, USA: Southern Research Station.

Weiskittel, A. R., D. W. Hann, J. A. Kershaw Jr, and J. K. Vanclay. 2011. *Forest Growth and Yield Modeling*. Oxford, UK: John Wiley & Sons.

White, J. C., N. C. Coops, M. A. Wulder, M. Vastaranta, T. Hilker, and P. Tompalski. 2016. "Remote Sensing Technologies for Enhancing Forest Inventories: A Review." *Canadian Journal of Remote Sensing* 42 (5): 619–641. doi:10.1080/07038992.2016.1207484.

White, J. C., M. Penner, and M. Woods. 2021. "Assessing Single Photon LiDar for Operational Implementation of an Enhanced Forest Inventory in Diverse Mixedwood Forests." *The Forestry Chronicle* 97 (01): 78–96. doi:10.5558/tfc2021-009.

White, J. C., P. Tompalski, M. Vastaranta, M. A. Wulder, N. Saarinen, C. Stepper, and N. C. Coops. 2017. *A model development and application guide for generating an enhanced forest inventory using airborne laser scanning data and an area-based approach*, FI-X-018. Victoria, BC, Canada: Natural Resources Canada. Accessed November 15, 2022. http://cfs.nrcan.gc.ca/publications?id=38945

Wulder, M. A., J. C. White, R. F. Nelson, E. Næsset, H. O. Ørka, N. C. Coops, T. Hilker, C. W. Bater, and T. Gobakken. 2012. "Lidar Sampling for Large-Area Forest Characterization: A Review." *Remote Sensing of Environment* 121: 196–209. doi:10.1016/j.rse.2012.02.001.

Wu, J., W. Yao, S. Choi, T. Park, and R. B. Myneni. 2015. "A Comparative Study of Predicting DBH and Stem Volume of Individual Trees in a Temperate Forest Using Airborne Waveform LiDar." *IEEE Geoscience and Remote Sensing Letters* 12 (11): 2267–2271. doi:10.1109/LGRS.2015.2466464.

Xiong, J. S., S. E. McKeand, R. W. Whetten, and F. T. Isik. 2014. "Genetics of Stem Forking and Ramicorn Branches in a Cloned Loblolly Pine Family." *Forest science* 60 (2): 360–366. doi:10.5849/forsci.12-018.

Yáñez, M. A., T. R. Fox, and J. R. Seiler. 2015. "Early Growth Responses of Loblolly Pine Varieties and Families to Silvicultural Intensity." *Forest Ecology and Management* 356: 204–215. doi:10.1016/j.foreco.2015.07.013.

Yáñez, M. A., J. R. Seiler, and T. R. Fox. 2017. "Crown Physiological Responses of Loblolly Pine Clones and Families to Silvicultural Intensity: Assessing the Effect of Crown Ideotype." *Forest Ecology and Management* 398: 25–36. doi:10.1016/j.foreco.2017.05.002.

Yao, W., P. Krzystek, and M. Heurich. 2012. "Tree Species Classification and Estimation of Stem Volume and DBH Based on Single Tree Extraction by Exploiting Airborne Full-Waveform LiDar Data." *Remote Sensing of Environment* 123: 368–380. doi:10.1016/j.rse.2012.03.027.

Yu, X., J. Hyyppä, M. Vastaranta, M. Holopainen, and R. Viitala. 2011. "Predicting Individual Tree Attributes from Airborne Laser Point Clouds Based on Random Forest Technique." *Isprs Journal of Photogrammetry and Remote Sensing* 66 (1, Jan): 28–37. doi:10.1016/j.isprsjprs.2010.08.003.

Yu, X., A. Kukko, H. Kaartinen, Y. Wang, X. Liang, L. Matikainen, and J. Hyyppä. 2020. "Comparing Features of Single and Multi-Photon Lidar in Boreal Forests." *Isprs Journal of Photogrammetry and Remote Sensing* 168: 268–276. doi:10.1016/j.isprsjprs.2020.08.013.

Zambrano, J., W. F. Fagan, S. J. Worthy, J. Thompson, M. Uriarte, J. K. Zimmerman, M. N. Umaña, N. G. Swenson, and P. Bellingham. 2019. "Tree Crown Overlap Improves Predictions of the Functional Neighbourhood Effects on Tree Survival and Growth." *The Journal of Ecology* 107 (2): 887–900. doi:10.1111/1365-2745.13075.

Zhang, W., J. Qi, P. Wan, H. Wang, D. Xie, X. Wang, and G. Yan. 2016. "An Easy-To-Use Airborne LiDar Data Filtering Method Based on Cloth Simulation." *Remote Sensing* 8 (6): 501. doi:10.3390/rs8060501.

Zhen, Z., L. J. Quackenbush, and L. Zhang. 2016. "Trends in Automatic Individual Tree Crown Detection and Delineation—Evolution of LiDar Data." *Remote Sensing* 8 (4): 333. doi:10.3390/rs8040333.